

RESEARCH

Open Access



# Palmitoyltransferase ZDHHC6 promotes colon tumorigenesis by targeting PPAR $\gamma$ -driven lipid biosynthesis via regulating lipidome metabolic reprogramming

Junqi Shan<sup>1†</sup>, Xinyu Li<sup>2†</sup>, Runqi Sun<sup>3†</sup>, Yao Yao<sup>1</sup>, Yan Sun<sup>4</sup>, Qin Kuang<sup>4</sup>, Xianling Dai<sup>4</sup> and Yanlai Sun<sup>1\*</sup>

## Abstract

**Background** The failure of proper recognition of the intricate nature of pathophysiology in colorectal cancer (CRC) has a substantial effect on the progress of developing novel medications and targeted therapy approaches. Imbalances in the processes of lipid oxidation and biosynthesis of fatty acids are significant risk factors for the development of CRC. Therapeutic intervention that specifically targets the peroxisome proliferator-activated receptor gamma (PPAR $\gamma$ ) and its downstream response element, in response to lipid metabolism, has been found to promote the growth of tumors and has shown significant clinical advantages in cancer patients.

**Methods** Clinical CRC samples and extensive in vitro and in vivo experiments were carried out to determine the role of ZDHHC6 and its downstream targets via a series of biochemical assays, molecular analysis approaches and lipid metabolomics assay, etc.

**Results** To study the effect of ZDHHC6 on the progression of CRC and identify whether ZDHHC6 is a palmitoyltransferase that regulates fatty acid synthesis, which directly palmitoylates and stabilizes PPAR $\gamma$ , and this stabilization in turn activates the ACLY transcription-related metabolic pathway. In this study, we demonstrate that PPAR $\gamma$  undergoes palmitoylation in its DNA binding domain (DBD) section. This lipid-related modification enhances the stability of PPAR $\gamma$  protein by preventing its destabilization. As a result, palmitoylated PPAR $\gamma$  inhibits its degradation induced by the lysosome and facilitates its translocation into the nucleus. In addition, we have identified zinc finger-aspartate-histidine-cysteine 6 (ZDHHC6) as a crucial controller of fatty acid biosynthesis. ZDHHC6 directly interacts with and adds palmitoyl groups to stabilize PPAR $\gamma$  at the Cys-313 site within the DBD domain of PPAR $\gamma$ . Consequently, this palmitoylation leads to an increase in the expression of ATP citrate lyase (ACLY). Furthermore, our findings reveals that ZDHHC6 actively stimulates the production of fatty acids and plays a role in the development of colorectal cancer. However, we have observed a significant reduction in the cancer-causing effects when the expression of ZDHHC6 is inhibited in in vivo trials. Significantly, in CRC, there is a strong positive correlation between the high

<sup>†</sup>Junqi Shan, Xinyu Li and Runqi Sun contributed equally to this work.

\*Correspondence:

Yanlai Sun

ylsun@sdfmu.edu.cn; sunyanlai@126.com

Full list of author information is available at the end of the article



© The Author(s) 2024. **Open Access** This article is licensed under a Creative Commons Attribution 4.0 International License, which permits use, sharing, adaptation, distribution and reproduction in any medium or format, as long as you give appropriate credit to the original author(s) and the source, provide a link to the Creative Commons licence, and indicate if changes were made. The images or other third party material in this article are included in the article's Creative Commons licence, unless indicated otherwise in a credit line to the material. If material is not included in the article's Creative Commons licence and your intended use is not permitted by statutory regulation or exceeds the permitted use, you will need to obtain permission directly from the copyright holder. To view a copy of this licence, visit <http://creativecommons.org/licenses/by/4.0/>. The Creative Commons Public Domain Dedication waiver (<http://creativecommons.org/publicdomain/zero/1.0/>) applies to the data made available in this article, unless otherwise stated in a credit line to the data.

expression of ZDHHC6 and the expression of PPAR $\gamma$ . Moreover, this high expression of ZDHHC6 is connected with the severity of CRC and is indicative of a poor prognosis.

**Conclusions** We have discovered a mechanism in which lipid biosynthesis is controlled by ZDHHC6 and includes the signaling of PPAR $\gamma$ -ACLY in the advancement of CRC. This finding provides a justification for targeting lipid synthesis by blocking ZDHHC6 as a potential therapeutic approach.

**Keywords** Colorectal cancer (CRC), ZDHHC6, PPAR $\gamma$ , Palmitoylation, Lysosomal degradation

## Introduction

Colorectal cancer ranks as the third most prevalent form of cancer in the population and is well recognized as a significant global public health concern. Colorectal cancer has the potential to metastasize from the colon's surface to the colon tissue and other organs such as the liver, prostate gland, seminal vesicle gland, and uterus if not detected early [1, 2]. While much research has been conducted on the molecular process behind the development of intestinal cancer, additional investigation is required to identify new and efficient therapeutic approaches. Recent epidemiological studies have discovered a connection between metabolic irregularities and numerous colon disorders, such as ulcerative colitis (UC), Crohn's disease (CD), and colorectal cancer (CRC) [3, 4]. The colon, being a crucial organ for metabolizing the three macronutrients, has been identified as playing a significant role in these diseases. It is important to mention that the worldwide occurrence of CRC is experiencing a significant rise, primarily attributed to the widespread problem of being overweight and the consequent emergence and advancement of obesity-related generalized metabolic syndrome [5, 6]. The lipid-rich state has a crucial role in promoting chronic inflammatory bowel disease (IBD) and colorectal cancer (CRC) driven by metabolic syndrome [7, 8]. Recent reports have extensively characterized the genetic changes in colorectal cancer (CRC), including mutations in TP53, KRAS, and EGFR [9, 10]. CRC is a very diverse malignancy with a low response to treatments and a high fatality rate. The etiology of colorectal cancer (CRC) and its related tumor formation is not yet fully comprehended, however disruption of genetic, immunological, and metabolic homeostasis is regarded to be crucial factors.

Metabolic reprogramming is primarily caused by the dysregulation of metabolic enzyme expression or activity. Palmitoylation is an essential posttranslational modification that controls the breakdown, location, and activation of metabolic enzymes in cells [11, 12]. It involves attaching fatty acids to substrate proteins. The disruption of palmitoylation is intricately linked to cellular lipid metabolism and facilitates the development and advancement of several types of malignancies, including colorectal cancer (CRC) [13]. Recently, there has been extensive research on a class of acyltransferases called

zinc finger-aspartate-histidine-cysteine (DHHC)-CRD-type palmitoyl acyltransferases (ZDHHCs) due to their probable involvement in stabilizing oncoproteins [14]. These enzymes have been investigated in several types of cancer. *S*-palmitoylation is a posttranslational modification that involves the attachment of C16 fatty acid palmitate (PA) to cysteine (Cys) residues of specific proteins [14, 15]. This process regulates the functionality of these proteins in different pathological and physiological situations. Significantly, palmitoylation has been found to regulate the specific localization and movement of proteins. This biological process relies on the catalytic activity of a sequence of palmitoyltransferases. ZDHHC2 and ZDHHC3, which are clearly described enzymes, have significant involvement in the process of lipogenesis [16, 17]. They directly palmitoylate and stabilize important lipogenesis components such as stearoyl-CoA desaturase (SCD), fatty acid synthase (FASN), and nuclear factor erythroid-2-related factor 2 (Nrf2) during carcinogenesis. ZDHHC6, a significant palmitoyltransferase, has been identified as a cancer signature gene and has high expression in various types of cancer [18–20]. ZDHHC6 primarily functions as an oncoprotein by increasing AEG-1 palmitoylation, which in turn activates or stabilizes transcription factors involved in cancer progression [21]. In addition, ZDHHC6 has a role in promoting cell proliferation by controlling the flow of calcium ions through selenium protein K during the development of tumor growth [22, 23]. Nevertheless, the role of ZDHHC6 in lipid metabolism is largely unknown.

Peroxisome proliferator-activated receptor gamma (PPAR $\gamma$ ) plays a crucial role in controlling lipid metabolism and energy balance, which are important biological processes involved in the advancement of colorectal cancer (CRC) [24, 25]. PPAR $\gamma$  has influence on diverse metabolic pathways and is present in colorectal epithelial cells, where its activation can stimulate cell differentiation and enhance apoptosis, therefore regulating tumor formation [26]. Moreover, PPAR $\gamma$  has been recognized as a crucial agent in the process of adipocyte differentiation, lipid storage, and glucose metabolism, all of which play a significant role in creating the tumor microenvironment and facilitating the survival of cancer cells [27, 28]. The abnormal lipid metabolism in cancer cells is currently acknowledged as a distinguishing feature of

cancer and has a substantial impact on facilitating rapid cell growth and spread to other parts of the body [29]. CRC cells frequently undergo significant modifications in both fatty acid synthesis and degradation, which play a role in membrane biosynthesis, energy storage, and signal transmission. These changes ultimately support the formation and progression of cancer. PPAR $\gamma$  agonists have been shown to inhibit the development of colon cancer, highlighting the receptor's potential as a target for therapeutic intervention in the treatment of colorectal cancer (CRC) [30, 31]. Changes in PPAR $\gamma$  expression and activity can influence the development of colorectal cancer (CRC) by changing the way lipids are processed, causing inflammation, and impacting insulin sensitivity. These factors are crucial for cancer cells to adapt and survive in the intestinal environment. Nevertheless, the precise involvement of PPAR $\gamma$  in cancer biology is not well understood. Recent research have shown that the process of phosphorylation of AKT stimulates the production of PPAR $\gamma$ , which in turn enhances the synthesis of lipids and the development of tumors in colorectal cancer (CRC) [32–34]. Our work revealed a correlation between the overexpression of ZDHHC6 and a substantial increase in lipid biosynthesis in CRC. We demonstrated that ZDHHC6 promotes the synthesis of fresh fatty acids and the formation of tumors by palmitoylating and stabilizing PPAR $\gamma$  in colon cancer. The results of our study offer a potential approach to specifically inhibit the production of fatty acids, which could have therapeutic advantages for individuals with elevated ZDHHC6 levels in colorectal cancer.

## Materials and methods

### Research consent and ethical statement

The experimental procedures involving animals in this study were conducted in accordance with the guidelines outlined in the Guide for the Care and Use of Laboratory Animals (1996, in Chinese). Additionally, these procedures were approved by the Institutional Animal Use and Care Committee at Shandong Cancer Hospital and Institute, Shandong First Medical University, and Shandong Academy of Medical Sciences in Jinan, China. The study recruited patients with colorectal cancer (CRC) phenotypes from the Department of Gastrointestinal Surgery and Clinical Trial Research Center at Shandong Cancer Hospital and Institute, Shandong First Medical University, and Shandong Academy of Medical Sciences (Jinan, China). The diagnosis of colorectal cancer (CRC) was established after a comprehensive evaluation that included radiologic, clinical, and endoscopic examinations, as well as careful analysis of histology data. The individuals included in this study had been diagnosed with Crohn's disease (CD), ulcerative colitis (UC), or colorectal cancer (CRC). The determination of ulcerative

colitis (UC) or Crohn's disease (CD) was achieved through the utilization of histological data in conjunction with radiologic, clinical, and endoscopic assessments. The specific attributes are outlined in Supplemental Tables 1 and 2. Each patient donor granted informed consent, and the research was approved by the Institutional Research Ethics Committee of Shandong First Medical University and Shandong Academy of Medical Sciences (Jinan, China).

### Identification of candidates

We screened candidate genes using the following procedures in order to find genes involved in the progression and metabolism of colorectal cancer (CRC): (1) Data Acquisition: The Cancer Genome Atlas (TCGA), International Cancer Genome Consortium (ICGC), and Gene Expression Omnibus (GEO) databases provided gene expression data and pertinent clinical information on CRC patients (GEO: GSE254054, GSE231943, GSE252858, GSE234804, GSE236678, GSE231436, GSE197088, and GSE239549). (2) Finding consistently differentially expressed genes (DEGs): In each data set, the function *t*-test in R was used to see if there was a significant difference in the level of gene expression between CRC tissues and adjacent or normal tissues. Benjamini-Hochberg correction was then applied. For the ensuing analysis, the lists of upregulated or downregulated DEGs in each of the ten datasets were utilized. (3) Candidate gene survival study in colorectal cancer: Clinical status and follow-up duration were taken from the clinical data of CRC patients. After excluding patients for whom there was no overall survival statistics or information, a survival analysis was carried out using the R packages "survival" and "survminer." (4) Gene set variation analysis (GSVA): The sample-wise biological processes of gene ontology (GO) activity variation were estimated using the GSVA R package. Single-sample GSVA scores were computed using a gene expression matrix, with each GO gene set including a minimum of ten genes. The GSVA scores of biological processes linked to cancer and the fold change in the expression levels of overlapping genes were analyzed using the Pearson correlation coefficient. (5) GSEA, or gene set enrichment analysis: In each dataset, CRC samples were compared to adjacent normal tissues using the GSEA software. The Molecular Signatures Database provided the gene set 'c5.all.v6.2.symbols.gmt', which was utilized in this investigation. Following the use of a 0.05 P value criterion and a 0.25 FDR threshold, the genes found were considered significant. Additionally, we ran GSEA on CRC tissues with high and low ZDHHC6 expression levels from the TCGA and ICGC databases.

### Cell culture

The human colorectal cancer cell lines SNU-C2A (Cat#: CCL-250.1), SW48 (Cat#: CCL-231), HT-29 (Cat#: HTB-38), LS1034 (Cat#: CRL-2158), HCT116 (Cat#: CCL-247EMT), Caco-2 (Cat#: HTB-37), and the FHC cells (Cat#: CRL-1831) derived from the human colon were acquired from the American Type Culture Collection (ATCC). The mouse-associated CRC cell lines, namely CT26 (Cat#: CRL-2638), MC38 (Cat#: CVCL\_B288), CMT93 (Cat#: CVCL\_1986), MC26 (Cat#: CVCL\_0240), and the normal mouse colon cell line MODE-K (Cat#: CVCL\_B4FG), were acquired from Cellosaurus. The entire cell line was discovered and confirmed to be devoid of mycoplasma. CRC cell lines were cultured in RPMI1640 medium (Cat#: LM87077C, LMAI Bio, China) supplemented with 10% premium quality fetal bovine serum (FBS) (Cat#: abs972, Absin, China) and 1×penicillin-streptomycin solution (Cat#: U31-301 C, YOBIBIO, China). The cells were cultured in culture plates at 37 °C in a humidified atmosphere with 5% CO<sub>2</sub>. The FHC or MODE-K cells were cultured in RPMI-1640 media supplemented with 10% fetal bovine serum (FBS), as specified in the product and instruction manuals. Following the transfection process, specific cells were placed in 6-well, 12-well, or 24-well plates with 60% fusion for 24 h prior to cell transfection. Subsequently, the cells were transfected using Convoy™ Transfection Reagent (Cat#: No. 11103, ACTGene Inc.) as instructed in the product description. Concisely, the transfection mixture was formulated by combining 2 µg of vector, 5 µl of Lipo3000 transfection reagent, and 120 µl of Gibco Opti-MEM™.

### Antibodies, chemicals and reagents

The corresponding primary antibodies used in this study were purchased from Abcam Inc<sup>®</sup>. The antibodies were specific to the following target proteins: ACTIN (Catalog number: ab179467, diluted at a ratio of 1/2500), PPAR gamma (Catalog number: ab272718, diluted at a ratio of 1/1000), PPAR delta (Catalog number: ab23673, diluted at a ratio of 1/1000), PPAR alpha (Catalog number: ab61182, diluted at a ratio of 1/1000), SREBP1 (Catalog number: ab28481, diluted at a ratio of 1/1000), Myc (Catalog number: ab32, diluted at a ratio of 1/1000), RAB11B (Catalog number: ab228954, diluted at a ratio of 1/150-1/1000), LAMP1 (Catalog number: ab24170, diluted at a ratio of 1/150-1/1000), Lamin B1 (Catalog number: ab229025, diluted at a ratio of 1/1000). The antibodies against ZDHHC6 (Catalog number: ABIN7162558, dilution ratio of 1/200–1/1000) and ZDHHC6 (Catalog number: ABIN6989238, dilution ratio of 1/200–1/1000) were acquired from antibodies-online in Limerick, PA, US. The antibodies against HA (Catalog number: 3724, diluted at a ratio of 1/250–1/1000) and Flag (Catalog number: 14793, diluted at a ratio of 1/250–1/1000) were

acquired from Cell Signaling Technology™ (CST). The supplementary anti-Na, K-ATPase antibody (Catalog number: H00000483-B01P) and PPARG antibody (Catalog number: NBP2-22106) were acquired from Novus Biologicals, LLC at a dilution ratio of 1/250-1/1000.

The protein concentration of the samples was determined using the BCA Protein Assay Kit (Catalog number: YSD-500T, Yoche-Biotech, China). The western blotting study employed HRP-tagged secondary antibodies (Catalog number: bs-0297 M-HRP, Bioss, China) at a dilution ratio of 1/15,000–1/20,000 for visualization purposes. The MG-132 (Catalog number: T2154) and cycloheximide (CHX) (Catalog number: T29590) were acquired from TargetMol Chemicals Inc., located in Shanghai, China. The compounds Biotin picolyl azide (Catalog number: 900912), alkynyl myristic acid (Alk14) (Catalog number: 1164), alkynyl palmitic acid (Alk16) (Catalog number: 1165), and alkynyl stearic acid (Alk18) (Catalog number: 1166) were acquired from Click Chemistry Tools. We synthesized and manufactured the alkynyl arachidic acid (Alk20) in our laboratory, achieving a purity level of above 98%. The compounds 2-bromopalmitate (2-BP) (Catalog number: 21604) and BSA (Catalog number: V900933) were acquired from Merck KGaA. The compound known as palmostatin M (Palm M) (Catalog number: 565407) was acquired from Med-Koo Biosciences, Inc. The TaqMan® Universal PCR Master Mix (Catalog Number: P/N4304437) and PowerUp™ SYBR™ Green (Catalog Number: A25742) were acquired from Applied Biosystems.

The pan palmitoylation-specific antibody was acquired as a generous gift from the research laboratory of Dr. Xu at the Chongqing University of Education [35]. In summary, to create an antibody that specifically targets pan palmitoylation, a brief peptide containing just two Cys C-C (pal) bonds (98.5% purity) was produced. One of the cysteine residues in the peptide was palmitoylated. This peptide was then utilized as the hapten, following established techniques and procedures. Subsequently, the acquired peptide C-C (pal) was linked with keyhole limpet hemocyanin (KLH) to serve as an extra antigen for the immunization of New Zealand white rabbits. The anti-serum was collected following the administration of three doses of passive immunization. Prior to utilization, employ ammonium sulfate precipitation for the purification of this anti-serum. In order to enhance the verification of this antibody, we have employed multiple supplementary validation methodologies. Essentially, the hydroxylamine buffer liquid can generate free sulfhydryl groups through the thioester linkages formed between the protein and palmityls. The TS-6B resin was employed to isolate the palmitoylated valosin-bearing protein that had been treated in a hydroxylamine buffer. Subsequently, an immunoblotting experiment was conducted

using an anti-valosin-bearing protein antibody. Additionally, the acquired antibody was subsequently employed to examine the palmitoylation of the short c-terminal domain phosphatase 1, as detailed in the prior investigation. In this study, the pre-existing antibody was used to examine the palmitoylated proteins obtained from cells treated with various drugs, including Palm B, Palm M, or 2-BP. The aforementioned techniques collectively enhanced the sensitivity and specificity of the antibody in detecting the protein palmitoylation process.

#### Knockout cell and knockdown lines preparation

The pre-existing system for generating knockout cell lines with targeted gene deficiencies, which is relevant to the ongoing research, was established as previously described. Essentially, a CRC cell line was created by using the CRISPR-Cas9 method to delete the *ZDHHC6* or *PPARG* genes. The pre-designed short guide RNA (sgRNA) targeting the human *ZDHHC6* or *PPARG* gene was generated and inserted into pLentiCRISPRV2-GFP vectors (#98290, Testobio Co., Ltd., China) to produce the CRISPR-Cas9 sgRNA-packaging lentivirus. The ready-made CRISPR/Cas9 KO products for human *ZDHHC6* plasmid (#sc-418298) and *PPAR $\gamma$*  plasmid (#sc-400030) were acquired from Santa Cruz Biotechnology, Inc. The sgRNA oligonucleotides were inserted into pLentiCRISPRV2 vectors that had been cleaved by the BsmBI restriction enzyme. The clones carrying gene deletions were extracted and identified using western blotting.

#### Plasmids and vectors preparation

The segments of DNA encoding the sgRNAs were inserted into PX330 (#PVT6301, Nova Lifetech Inc.) in order to introduce the N-terminal S-protein-Flag-Streptavidin binding peptide (SFB) tag at the endogenous *ZDHHC6* gene location. The donor vector for *ZDHHC6* knock-in was created using Gibson assembly of 50 homologous arms, Puro-P2A-SFB, and 30 homologous arms into the pUC19 plasmid (#N3041L, New England Biolabs). The *ZDHHC6* open reading frames of human origin were produced using PCR amplification using complementary DNA derived from HCT116 cells. In addition, full-length *Homo sapiens ZDHHC6* cDNA plasmids were created using PCR-based cDNA amplification. These plasmids were then inserted into pcDNA3.4™ TOPO™ plasmids (#A14697, Thermo Fisher Scientific Inc.) that were tagged with either 3×HA or 3×Flag for use in other in vitro investigations. Expression vectors containing shortened fragments of the *PPARG* gene, such as Myc-PPARG WT, Myc-PPARG-AF1, Myc-PPARG-DBD, and Myc-PPARG-hinge-LBD, were generated as planned. In addition, to further investigate the functional impacts of *ZDHHC6* in laboratory conditions, targeted protein expression vectors were created by loading adenoviruses

with the use of a pre-made adenovirus packaging kit (Haixing Biosciences, Suzhou, China). The complete *Homo sapiens ZDHHC6* cDNA plasmids and their corresponding ready-made shRNA targeting human *ZDHHC6* (sh*ZDHHC6*), shRNA targeting human *PPARG* (sh*PPARG*), human *PPARG* sequences with the C313S mutant, and *Homo sapiens* full-length *PPARG* sequences were individually packaged into adenovirus using a commercially available adenovirus packaging kit (Haixing Biosciences, Suzhou, China). The adenovirus particles were purified and quantified to a titer of  $6.0 \times 10^{10}$  PFU using the Adenovirus Purification Mini Kit (#V1160-01, Shanghai Juncheng Biotechnology, China) following the instructions provided in the operation handbook.

#### Histological analysis

The histopathologic assay was conducted by fixing the cells or tumor tissue with a 4% formaldehyde solution called Image-iT™ (#R37814, Thermo Fisher Scientific Inc.), and thereafter cutting it into transverse sections. The cell slices were subjected to treatment with the specified primary antibodies at a temperature of 4 °C for a duration of 24 h. The Leica DM IL LED microscope was used to capture histological pictures for examining specimen sections, while a confocal laser microscopy system (Olympus, Japan) was used for investigating immunofluorescence sections after incubating them with the appropriate secondary antibodies. The tumor specimens were immersed in a 4% formaldehyde solution for 24 h to preserve them, and subsequently embedded in an OCT (optimal cutting temperature) compound. The embedded tissues were sliced into sections of 20 micrometers in thickness. Xylene was employed for the purpose of eliminating the paraffin from the tissue sections during the process of IHC staining, followed by subsequent rehydration. Subsequently, they were immersed in a solution containing 5% normal target serum and 3% BSA (Beyotime) for a duration of 1.5 h. The specified primary antibodies were introduced and left to incubate overnight at a temperature of 4 °C. Following the washing step, a 1:300 dilution of HRP-conjugated secondary antibody (Abcam) was applied and incubated for 1 h. The DAB substrate was introduced to analyze the signals. Photographs were taken with a light microscope.

#### Immunoprecipitation and S-protein pull down assay

Immunoprecipitation and SFB pull-down experiment was performed as described previously [42]. Briefly, cells were lysed in E1A lysis buffer (250 mM NaCl, 50 mM HEPES [pH 7.5], 0.1% NP-40, 5 mM EDTA, protease inhibitor cocktail [Sigma]). The antibodies to *ZDHHC6* were used for immunoprecipitation. HCT116 cells were transfected with SFB-tagged protein and lysed in NETN buffer (200 mM Tris-HCl [pH 8.0], 100 mM NaCl, 0.05%

NP-40, 1 mM EDTA, protease inhibitor cocktail [Sigma]) for 20 min at 4 °C. Crude lysates were subjected to centrifugation at 14,000 × g for 15 min at 4 °C. Supernatants were incubated with S-Protein Agarose for 4 h (Millipore, USA). The agaroses were washed three times with NETN buffer. Proteins were eluted by boiling in 1× SDS loading buffer and subjected to SDS-PAGE for immunoblotting.

#### GST pull-down assay

GST pull-down assay was used to detect the direct interaction between PPAR $\gamma$  and ZDHHC6. Briefly, GST-tagged PPAR $\gamma$  (GST-PPAR $\gamma$ ) and 6×His-tagged ZDHHC6 (His-ZDHHC6) or 3×Flag-tagged ZDHHC6 (Flag-ZDHHC6) proteins were expressed in BL21 (DE3) *Escherichia coli* via transforming pGEX-4T-1-GST-PPAR $\gamma$  and pET24a-His-ZDHHC6 or pET24a-Flag-ZDHHC6 plasmids, respectively. Then, the *E. coli* were collected, sonicated, and purified with cOmplete His-Tag Purification Resin (Roche) or Purification of Flag kit (Sigma-Aldrich) to obtain purified ZDHHC6-tagged protein. GST-PPAR $\gamma$  protein was expressed and immobilized with BeyoGold™ GST-tag Purification Resin (Beyotime) following the manufacturer's instructions. The beads-PPAR $\gamma$  complexes were washed with GST pull-down binding buffer (50 mM Tris-HCl, 200 mM NaCl, 1 mM EDTA, 1% NP-40, 1 mM DTT, 10 mM MyCl<sub>2</sub>, pH 8.0) and incubated with purified ZDHHC6-tagged protein at 4 °C for 4 h on a rotating windmill. Finally, the beads were washed and analyzed by immunoblotting assay.

#### Quantitative PCR (qPCR) assay

The cells or tissue RNA were obtained and isolated using TRNzol universal reagent (#DP405-02, TIANGEN Biotech Co., Ltd., Beijing) following the instructions provided in the operating handbook. The pre-prepared RNA samples were stored in a refrigerator at a temperature of -80 °C for a maximum of 10 days (#TSX40086V, Thermo Fisher Scientific Inc.). The optimal RNA purity was assessed based on the observation of an absorption ratio (values > 2.00) at 260/280 nm. Subsequently, 1.5  $\mu$ g of pure RNA was subjected to reverse transcription using the PrimeScript™ RT-PCR Kit (#RR014A, Takara) and the Fast PCR Master Mix (#HY-K0532, MedChem-Express, Beijing). The reverse transcription process was conducted at a temperature of 42 °C for a duration of 1 h, and subsequently, the enzyme was deactivated at a temperature of 70 °C for a period of 10 min. The PCR procedure was conducted utilizing SYBR Green qPCR Master Mix (#HY-K0501, MedChemExpress, Beijing) and SYBR qPCR Master Mix (Universal) (#22204, ToloBio, China) on QuantStudio 7 Pro equipment (Applied Biosystems). The pre-designed, precise primer sequences were acquired from OriGene Technologies, Inc.

#### Western blotting assay

In order to conduct the western blotting assay, the materials were prepared by homogenizing them with a commercially available RIPA lysis buffer solution (#BL504A, Biosharp, Shanghai, China). Subsequently, the ultimate homogenized extraction was condensed using centrifugation at a temperature of 4 °C and a speed of 13,000 rpm for a duration of 30 min. The protein samples obtained were standardized using the BCA Protein Assay Kit (Catalog number: YSD-500T, Yoche-Biotech, China), using lipid-free BSA as the control. The cell lysis samples were analyzed using a 12% ShineGel™ Plus Tris-Glycine PAGE kit (#SP0511, Shinegene, China) and transferred onto a 0.45  $\mu$ m hydrophobic polyvinylidene fluoride transfer membrane (#IPFL00010, Sigma-Aldrich). Immunoblotting was performed using the specified primary antibodies. Afterwards, the PVDF membranes were subjected to treatment with Western Blocker™ buffer in a working solution of 1×TBS, which included 0.1% Tween-20 (#T104863, Aladdin, China), for a duration of 1 h. Subsequently, the membranes were incubated with the designated primary antibodies at a temperature of 4 °C for a period of 24 h. The PVDF membranes used in Western blotting were subjected to exposure using the ECL Plus kit test (#E266188, Aladdin, China) and subsequently exposed to medical X-ray film (Blue Ocean Imaging Systems, China). The protein contents were quantified as gray value levels using Image J, version 1.8.0, and then normalized to ACTIN as a fold change.

#### Labelling, click chemistry, and palmitoylation identification

The Click-iT™ Palmitic Acid (PA), Click-iT™ Cell Reaction Buffer Kit (#C10269), Click-iT™ Protein Reaction Buffer Kit (#C10276), and Azide Kit (#C10265) were acquired from Invitrogen for the purpose of conducting click chemistry and identifying palmitoylated PPARG, following the instructions provided with the products. Following the specified transfection of PPARG WT and PPARG C313S mutants, the cell media was treated with 100  $\mu$ m Click-iT PA, azide, and kept in a 5% CO<sub>2</sub>, 37 °C environment for 5 h. After a treatment duration of 5 h, the cells were collected and subsequently rinsed four times with pre-cooled D-PBS (#abs9340, Absin, China). This was followed by a combination with lysis buffer containing 1×protease and a general phosphatase inhibitor cocktail (#abs9162, Absin, China). The lysates were thereafter kept at a temperature of 4 °C for a duration of 40 min, after which they were transferred to a centrifugal tube with a volume of 2 ml. The ultimate cell lysates were condensed using centrifugation at a temperature of 4 °C and a speed of 13,500 revolutions per minute for a duration of 10 min. The protein concentration of the collected supernatant was verified using the EZQ™ Protein Quantitation Kit (#R33200, Thermo Fisher Scientific) following

the instructions provided in the product manuals. The extracted proteins were incubated with biotin-alkyne using the Click-iT™ Protein Reaction Buffer Kit, following the protocols outlined in the production instruction specification. Subsequently, the biotin-alkyne-palmitic acid and azide-protein complexes were subjected to streptavidin-mediated pulldown experiments using streptavidin magnetic beads (#HY-K0208, MedChemExpress, China). The resulting samples were then analyzed by western blotting using the PPAR $\gamma$  antibody.

Furthermore, to enhance the identification of the palmitoylation of PPAR $\gamma$ , an additional complementary approach was employed in this section. The cells were treated and lysed using a buffer containing 1% Triton X-100, 150 mM NaCl, 0.2% SDS, 50 mM TEA-HCl at pH 7.4. The buffer also contained 1 $\times$ protease and phosphatase inhibitor cocktail. Additionally, a click reaction with biotin azide was performed. The cell proteins were extracted using 10 volumes of 100% methyl alcohol at a temperature of -80 °C for a duration of 1.5 h. Subsequently, the proteins were collected again by centrifugation at a speed of 13,500 revolutions per minute for a period of 15 min. The precipitates were resuspended in 100 ml of a 1 $\times$ suspension buffer and subsequently diluted to a 12-fold immunoprecipitation solution. The immunoprecipitation solution consisted of 0.5% Nonidet P 40, 55 mM Tris-HCl, 160 mM NaCl, 6.5 mM EDTA, and had a pH of 7.5. The cell proteins that were marked with labels were concentrated using streptavidin agarose at a temperature of 30 °C, with a gentle swirling motion for a duration of 1.5 to 2.0 h. The protein-bound streptavidin agarose beads underwent four washes using an immunoprecipitation solution. Subsequently, the protein-bound beads were released using an elution buffer consisting of 95% formamide and 10 mM EDTA with a pH of 8.2, heated to 95 °C for a duration of 5 min. The samples were then analyzed using immunoblotting detection.

#### Fractionation assay

The separation of components was achieved using the Nuclear/Cytosol Fractionation Kit (#K266-100, BioVision, US) or Nuclear/Cytosol Extraction Kit (#ab289882, Abcam). The nuclear component was disrupted using a homogenization solution consisting of 5% SDS, 1 $\times$ protease inhibitor cocktail, 2.5 mM PMSE, 160 mM NaCl, 60 mM triethanolamine, 1600 units/ml benzonase nuclease, pH 7.5. After removing the solution, a final homogenization of 6.5 mM was achieved by adding EDTA. Prior to the subsequent fractionation assay, the cytoplasmic component was diluted using a homogenization solution that contained 6 mM EDTA.

#### Cell proliferation detection

The CCK-8 assay was used to measure the proliferation of cancer cells. The cultured cells were placed in a 96-well plate and incubated for different lengths of time, with a density of  $2.5 \times 10^4$  cells per well. After each treatment, the liquid above the culture was removed, and 15  $\mu$ l of Cell Counting Kit-8 (CCK-8) from ApexBio Technology (#K1018) was added to each well. After being kept at a temperature of 37 °C for 2 h, the fluorescence intensity at a wavelength of 450 nm was quantified using a microplate reader. Colony formation was utilized as a technique to examine cell proliferation. To summarize, the designated cancer cells were inserted in a 24-well plate, with each well containing 200 cells. Following a period of 2 weeks, colonies with a cell count exceeding 50 were visually observed and measured using crystal violet staining.

#### Transwell assay

Cell migration and invasion were quantified using Transwell assay. The Corning® Transwell® (#CLS3422, Corning, USA) was cultured with Matrigel (#356234, BD, USA). The tumor cells that were identified were cultivated again in a medium without serum (#12-725 F, LONZA, USA) and then placed in the upper chamber with a density of  $6.0 \times 10^4$  cells per well. Subsequently, the medium containing 10% fetal bovine serum (FBS) was introduced into the bottom chamber, and then administered for a duration of 48 h. Subsequently, the cells in the top chamber were entirely eliminated by means of a cotton swab. The cells that moved into the lower chamber were washed, treated with a 4% formaldehyde solution to preserve them, and then colored with a 0.65% crystal violet stain. Finally, the cells were visualized using a microscope. The migration calculation experiment was conducted using identical techniques, with the exception that Matrigel was omitted during the pre-coating of the upper chamber.

#### In vivo xenograft models construction

Pathogen-free male BALB/c nude mice (5 weeks old, 20–22 g, Beijing Vital River Laboratory Animal Technology Co., Ltd., Beijing, China) underwent a subcutaneous procedure in the flank region, where  $1.6 \times 10^6$  HCT116 or SNU-C2A cells were injected in a suspension of 80  $\mu$ l PBS. The mice were split into treatment groups at random once the xenograft tumors reached the expected volume. Tumor dimensions were measured at regular intervals of 2–3 days using a vernier caliper. The tumor's volume was determined by applying the formula  $1/2 \times D$  (major axis)  $\times d^2$  (minor axis). Mice were euthanized without causing pain after the tumor size reached 2 cm<sup>3</sup> or when ulceration was detected. All animal experimental protocols were performed following the Ethical

Animal Care and Use Committee of Shandong University (2021sa0541jk).

#### **Triglyceride detection and lipid accumulation in vitro assay**

The measurement of TG was conducted using the Triglyceride Quantification Kit (#K622-100, BioVison, US). A total of  $6 \times 10^5$  cells were gathered and subsequently combined with 1 ml of extraction reagent. The samples were subjected to ultrasonic treatment for a duration of 1 min, followed by centrifugation at a speed of  $9000 \times g$  at a temperature of  $4^\circ\text{C}$  for a duration of 10 min. The liquid portion was collected for analysis in accordance with the guidelines provided by the manufacturer. The Green Fluorometric Lipid Droplet Assay Kit (BODIPY-493/503) was employed to detect lipid deposition in CRC cells. This kit allowed visualization of the production of lipid droplets in the specified in vitro tests.

#### **RNA sequencing**

The TRNzol universal reagent was used to extract RNA from HCT116 cells, following the manufacturer's procedure. The quantification of RNA samples was performed using the BioPhotometer Plus (Eppendorf), while the assessment of RNA integrity was conducted using the Agilent 2100 bioanalyzer system. The Collibri Stranded RNA Library Prep Kit for Illumina, provided by Thermo Fisher Scientific, was utilized for RNA sequencing library preparation, following the instructions provided by the vendor. The sequencing process was performed on the Illumina HiSeq instrument utilizing a  $2 \times 150$  Paired End configuration, with 35 million reads obtained per sample by GENEWIZ, LLC. The construction of sequencing libraries was performed using the Small RNA-Seq Library Prep Kit (#052.08, Lexogen GmbH, Vienna, Austria) with total RNA as the starting material. In summary, the messenger RNA (mRNA) was extracted from the whole RNA using Sera-Mag SpeedBead particles and subsequently subjected to chemical fragmentation. The RNA fragments were subjected to reverse transcription, where they were converted into complementary DNA (cDNA) using random primers that had a tagging sequence attached to their 3' ends. The cDNA libraries were subsequently amplified using the KAPA high-fidelity DNA polymerase. The validation of the libraries' quality was conducted using the Agilent 2100 bioanalyzer. Following that, a high-throughput sequencing procedure was carried out utilizing an Illumina NovaSeq 6000. Following the mapping of sequences using the STAR or HISAT2 software against *Homo sapiens* or *Mus musculus*, a biological pathway analysis was conducted using Cluster-Profiler. The RNA sequencing and library creation were carried out

by the technical personnel at Nanjing Biomed Sciences Research Bio-Lab.

#### **Metabolomics and lipidomics assay**

Approximately 30 milligrams of tissues were combined with 550  $\mu\text{L}$  of a 75% methanol buffer to extract metabolites. The liquid portion was collected and subjected to lyophilization. The freeze-dried powder was dissolved in 60  $\mu\text{L}$  of 80% methanol. Following centrifugation, the liquid remaining after sedimentation, known as the supernatant, can be used for analysis with the TSQ Fortis Plus (#TSQ03-10003, Thermo Fisher Scientific)-Orbitrap Astral High Resolution MS (Thermo Fisher Scientific). The process of extracting metabolites from cells involved the following steps: Firstly, cells collected in a 10-cm dish were washed with pre-cooled PBS and immediately frozen using liquid nitrogen. The cells were subsequently disrupted using 1.5 mL of 80% methanol solution containing internal standards, and then removed from the dish by scraping. The liquid portion obtained after spinning the mixture at high speed and removing the solid particles was preserved. This liquid was then subjected to a process of removing moisture by freezing and subsequent drying. The resulting dried material was used for the examination of small molecules involved in metabolism using a technique called liquid chromatography-mass spectrometry (LC-MS). The process of extracting lipids from cells was conducted as follows: briefly, cells that were gathered in a 10-cm dish were washed with PBS and immediately frozen using liquid nitrogen. The cells were subsequently disrupted using 1.5 mL of methanol containing internal standards, combined with 1.5 mL of chloroform, and vigorously mixed for 30 s using a vortex. Afterward, 500  $\mu\text{L}$  of water were added and vortexed for an additional 30 s. The layer that repels water was gathered and subjected to freeze-drying. The dehydrated powder was reconstituted in 40  $\mu\text{L}$  of an organic solvent mixture (Chloroform: Methanol, 2:1) using a vortex for 30 s, and then combined with 70  $\mu\text{L}$  of another organic solvent mixture (Acetonitrile: Isopropanol: Water, 13:6:1). Following centrifugation, the liquid portion can be specifically utilized for TSQ Fortis Plus-Orbitrap Astral MS analysis.

#### **Glucose [ $U\text{-}^{13}\text{C}$ ] tracer assay**

The medium was replaced with RPMI 1640 supplemented with glucose (2 g/L) labelled with [ $U\text{-}^{13}\text{C}$ ] when the cell density reached around 80%. After 24 h, the cell culture plates were rinsed with PBS, rapidly frozen in liquid nitrogen, and kept at a temperature of  $-80^\circ\text{C}$ .

### Statistical analysis

The data were expressed as the mean  $\pm$  SEM (standard error of the mean) of three independent experiments conducted in triplicate. The software GraphPad Prism 8.0, developed by GraphPad Software in San Diego, USA, was utilized for the purposes of creating visual representations and doing statistical analysis. Unpaired Student's t-tests were employed to compare the two groups. A unidirectional analysis of variance (ANOVA) was conducted, followed by a Bonferroni post-hoc test to compare different groups. A *P* value less than 0.05 was deemed to be statistically significant. The scientists were unaware of the animal genotype and grouping information.

## Results

### Identification of potential genes strongly associated with the course and prognosis of colorectal cancer (CRC)

We examined the expression matrix of colorectal cancer and adjacent healthy tissues in public datasets that included high-coverage gene profiling data in the TCGA, ICGC, and NCBI Gene Expression Omnibus (GEO) databases (GEO: GSE254054, GSE231943, GSE252858, GSE234804, GSE236678, GSE231436, GSE197088, and GSE239549) in order to identify intriguing genes that regulate the progression of colorectal cancer (Fig. 1A). The CRC tissues exhibited a substantial enrichment of events linked to tumors and processes related to metabolism (Fig. 1B). Across the ten datasets we selected, we identified 41 differentially expressed genes (DEGs) that were conservatively upregulated and 101 DEGs that were downregulated (Fig. 1C). Notably, based on clinical data from the TCGA and ICGC databases, 6 upregulated and 4 downregulated DEGs were identified because they showed a substantial correlation with survival rates (Fig. 1D). Additionally connected to molecular processes influencing the development of colorectal cancer and metabolic reprogramming are these 6 upregulated and 4 downregulated DEGs (Fig. 1E).

Of the top four elevated DEGs most closely connected with CRC occurrences, we concentrated on ZDHHC6, the sole gene having the most underappreciated biological significance in CRC (Fig. 1E). Using the TCGA and ICGC datasets, we further confirmed that CRC had higher levels of ZDHHC6 expression than surrounding tissues (Fig. 1F, G). The samples in the TCGA and ICGC databases were split into two groups based on the ZDHHC6 expression value: one group was ZDHHC6 high-expression, and the other ZDHHC6 low-expression. Crucially, compared to those with low ZDHHC6 expression levels, those with high ZDHHC6 expression levels had a noticeably worse survival prognosis (Fig. 1H). There were significantly more biological processes associated with cancer growth and metabolic reprogramming

in the group with high ZDHHC6 expression on a regular basis. This demonstrated that ZDHHC6 is potentially associated with biological processes of CRC (Fig. 1I).

In addition, we examined the potential involvement of ZDHHC6 expression in colitis and the advancement of colorectal cancer (CRC) related with colitis, by analysing the intersection of ZDHHC6 in many datasets. Colon samples obtained from persons diagnosed with Crohn's disease (CD), ulcerative colitis (UC), and colorectal cancer (CRC), as well as from healthy donors (HC), exhibited markedly elevated levels of ZDHHC6 protein compared to the healthy individuals in the control group. This was particularly accurate for individuals with symptoms of ulcerative colitis (UC) and Crohn's disease (CD). Individuals exhibiting characteristics of colorectal cancer (CRC) demonstrated elevated levels of ZDHHC6 protein content in comparison to those in the Crohn's disease (CD), ulcerative colitis (UC), and healthy control (HC) groups (Supplementary Fig. 1A). The Pearson multiple correlation and multiple linear regression analyses demonstrated a positive correlation between ZDHHC6 protein levels and plasma concentrations of ESR, CRP, and ProCT. These laboratory markers are commonly used in the diagnosis of clinic colitis (Supplementary Fig. 1A, B). Significantly, we also verified a negative correlation between the levels of albumin (ALB) in the bloodstream, a potential indicator of inflammatory bowel disease (IBD), and the levels of ZDHHC6 in the colon. The results suggest a link between inflammatory bowel disease (IBD) and the concentrations of ZDHHC6 in the tissue of the colon (Supplementary Fig. 1A, B). A similar observation was documented in mice with colitis caused by dextran sulphate sodium (DSS), a frequently employed chemically-induced experimental model for colitis. Also, a notable elevation in ZDHHC6 protein levels as the disease advanced, as observed using the western blotting experiment (Supplementary Fig. 1C). Furthermore, considering the various physical characteristics and underlying factors that worsen both sudden and long-lasting inflammation of the colon, the objective of this study was to investigate whether changes in ZDHHC6 expression played a role in the advancement of colorectal cancer (CRC) and the development of chronic colitis caused by DSS. The control mice were given AOM+DSS treatment for a period of ten weeks to promote the onset of colitis-associated carcinogenesis (Supplementary Fig. 1D). Not surprisingly, there was a noticeable and significant increase in ZDHHC6 expression in colon samples from the mouse model with the CRC phenotype (Supplementary Fig. 1D). These findings indicated that abnormally upregulated ZDHHC6 levels are correlated with the severity of colitis and the development of CRC.

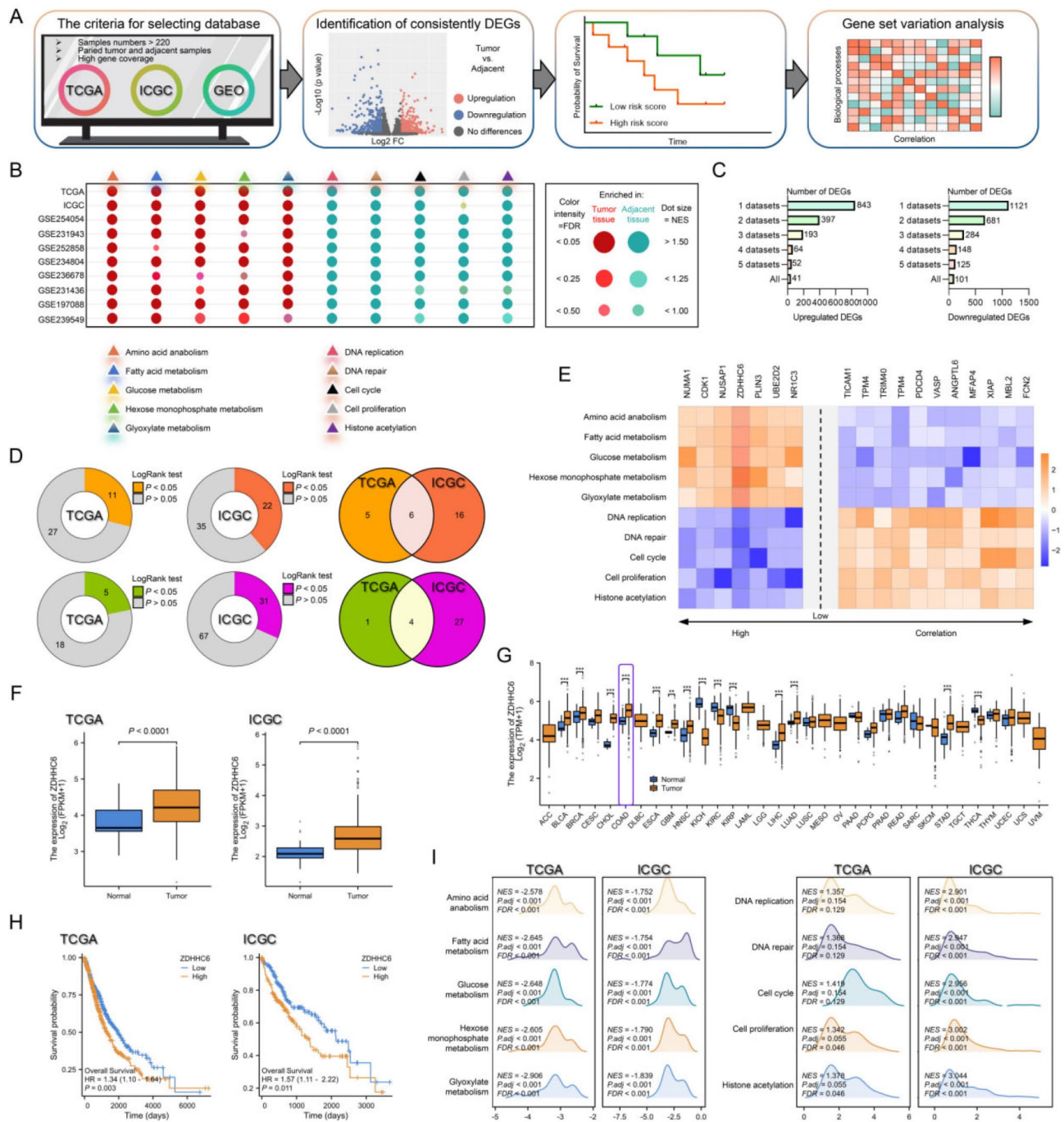


**Fig. 1** Identification of potential genes implicated in colorectal cancer (CRC) and cancer metabolism-associated biological processes. **(A)** A screening procedure to find putative gene candidates. **(B)** Colorectal cancer (CRC) samples were found to differ from adjacent controls in terms of physiopathology and biological processes related to metabolism in a number of databases, including TCGA, ICGC, and the NCBI Gene Expression Omnibus (GEO) datasets (GEO: GSE254054, GSE231943, GSE252858, GSE234804, GSE236678, GSE231436, GSE197088, and GSE239549). **(C)** Following gene differential expression analysis, the total number of differentially expressed genes that crossed over into various databases was counted. **(D)** Six upregulated and four downregulated DEGs were identified based on a survival analysis of differentially expressed genes across six databases. In the databases of TCGA and ICGC,  $P < 0.05$  was deemed statistically significant. **(E)** Six upregulated and four downregulated DEGs represent the molecular mechanisms impacting the onset of colorectal cancer and metabolic reprogramming. **(F)** Palmitoyltransferase ZDHHC6 expression in the ICGC and TCGA databases. **(G)** Pancarcinoma analysis using TCGA datasets to measure ZDHHC6 expression levels in various malignancies. **(H)** The overall survival (OS) of colorectal cancer patients in the TCGA and ICGC databases according to different ZDHHC6 expression levels. **(I)** After dividing the TCGA and ICGC samples' ZDHHC6 expression levels into groups of high and low expression levels, the grouped samples underwent GSEA analysis. The data were expressed as the mean  $\pm$  SEM. A P value less than 0.05 was considered statistically significant. \*\*\* $P < 0.001$

### Disturbed lipid metabolism in human CRC with upregulated ZDHHC6 levels

In addition to the substantial rise in ZDHHC6 observed in the TCGA dataset (Fig. 1G) and the ICGC database (Supplementary Fig. 2A), In order to confirm the increased expression of ZDHHC6 in colorectal cancer (CRC), we obtained 73 pairs of CRC samples and their matching adjacent samples. Our analysis revealed a significant increase in the mRNA expression levels of ZDHHC6 in CRC tissues compared to nearby normal tissues (Fig. 2A). In addition, the analysis of proteins revealed that both human CRC tumour tissues

and CRC-related cell lines (SNU-C2A, SW48, HT-29, LS1034, HCT116, and Caco-2) as well as mouse-associated colon cancer cell lines (CT26, MC38, CMT93, and MC26) exhibited elevated levels of ZDHHC6 expression. This finding was further validated through western blotting and immunofluorescence detection (Fig. 2B-E, Supplementary Fig. 2B). Hence, we examined potential processes that could contribute to the overexpression of ZDHHC6 in colorectal cancer (CRC). Subsequently, we identified the changes in its expression profile when exposed to 2-bromopalmitate (2-BP), a broad inhibitor of protein palmitoylation. The ZDHHC6 protein expression

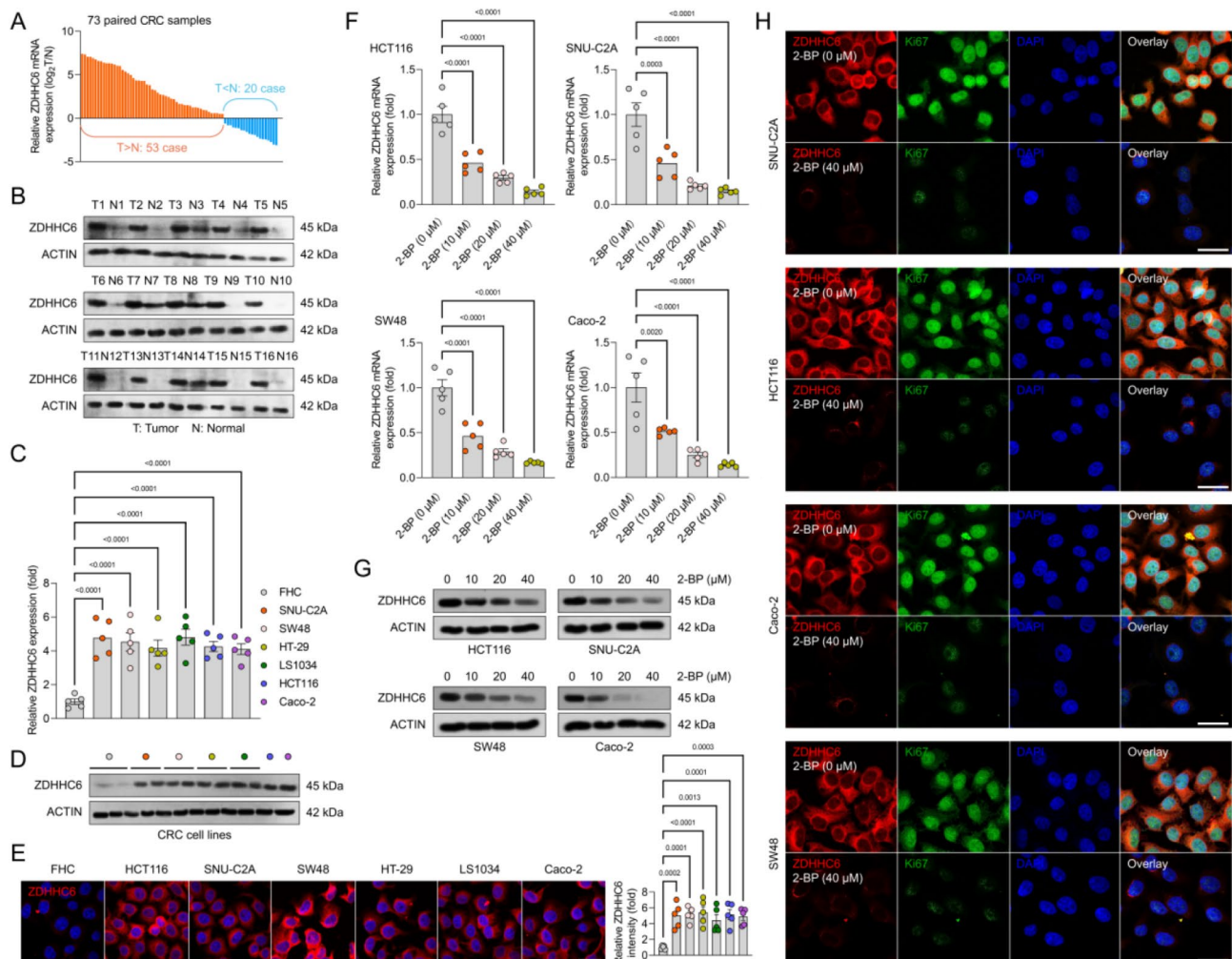


**Fig. 2** Increased ZDHHC6 is positively associated with the development of human colorectal cancer (CRC). **(A)** ZDHHC6 mRNA expression levels in 73 pairs of CRC sample pairs (T) and their corresponding adjacent sample pairs (N).  $n = 73$  pairs. **(B)** ZDHHC6 protein expression levels in sixteen pairs of similar adjacent tissues and colorectal cancer tissues selected at random. For each group,  $n = 3$ . **(C)** ZDHHC6 mRNA expression levels in relation to a range of CRC-associated cell lines, such as SNU-C2A, SW48, HT-29, LS1034, HCT116, and Caco-2, as well as the matching human normal colonic epithelial cell line (FHC), are displayed in qPCR analysis. For each group,  $n = 5$ . **(D, E)** ZDHHC6 protein expression in SNU-C2A, SW48, HT-29, LS1034, HCT116, Caco-2, and FHC cell line as demonstrated by western blotting **(D)** and immunofluorescence analysis **(E)**. 200  $\mu\text{m}$ ; each group has  $n = 5$ . **(F, G)** qPCR analysis **(F)** and western blotting experiment **(G)** demonstrate the effect of the gradually increased dosage of 2-bromopalmitate (2-BP) on the relative ZDHHC6 mRNA and protein expression levels in HCT116, SNU-C2A, SW48, and Caco-2 cell lines. For each group,  $n = 3$ . **(H)** An immunofluorescence assay demonstrating the co-expression of ZDHHC6 and Ki67 in response to 40  $\mu\text{M}$  2-bromopalmitate (2-BP) in HCT116, SNU-C2A, SW48, and Caco-2 cell lines. 200  $\mu\text{m}$ ; each group has  $n = 3$ . Data are expressed as mean  $\pm$  SEM. The relevant experiments presented in this section were performed independently at least three times.  $P < 0.05$  indicates statistical significance

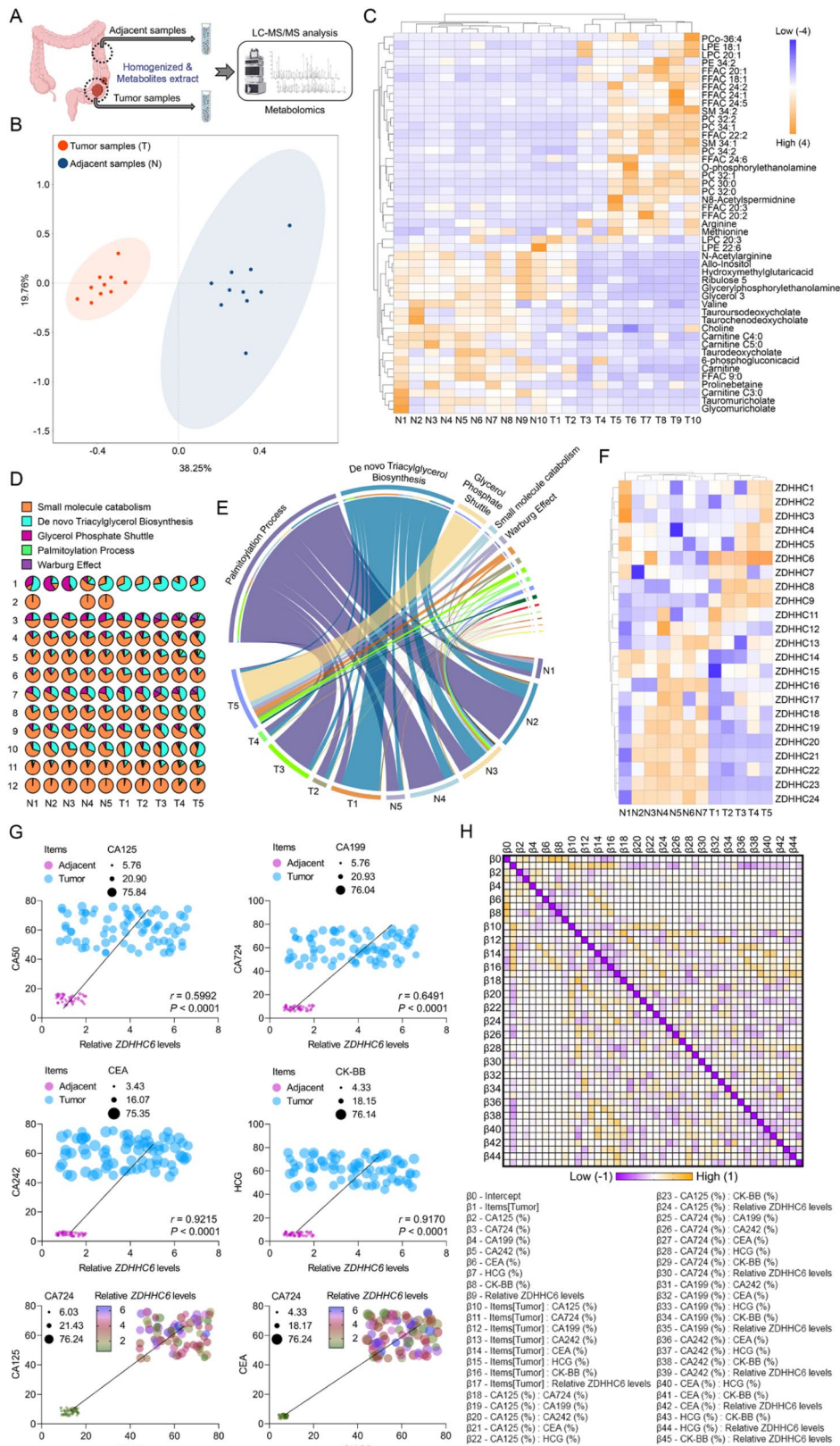


**Fig. 3** (See legend on next page.)

(See figure on previous page.)

**Fig. 3** Upregulated ZDHHC6 levels contribute to disturbed lipid metabolism in human colorectal cancer (CRC). **(A)** To identify significantly altered metabolites in ten pairs of colorectal cancer (CRC) samples and adjacent normal samples from CRC patients, a high-throughput LC-MS-based untargeted metabolomic analysis was carried out. Postoperative pathology confirmed that all patients had colorectal cancer; no other cancers or long-term medical problems were present. **(B)** The selected ten pairs of colorectal cancer (CRC) samples and adjacent normal samples from CRC patients were subjected to principal component analysis (PCA). **(C)** Heatmap of tumor samples (T) with significantly altered metabolites compared to corresponding normal adjacent tissue (N). Significant changes have been observed in 39 metabolites in cancerous tissues. Wilcoxon test with paired two-samples,  $P < 0.05$ . The fold change is indicated by  $-2.0 \sim 2.0$  (Fc). **(D)** Based on 39 significantly changed metabolite clusters discovered by pathway analysis (<https://www.metaboly.com/>), the pie chart illustrates the improved metabolic signaling pathways. **(E)** A chord diagram shows the direction and distribution of data flow as well as the relationships between different metabolic signaling pathways. **(F)** Heatmap analysis of the ZDHHCs protein expression fold change (T/N) in the normal adjacent samples and the CRC samples. Wilcoxon test with paired two-samples,  $P < 0.05$ . The fold change is indicated by  $-2.0 \sim 2.0$  (Fc). **(G)** The levels of ZDHHC6 protein and several tumor markers, such as CA125, CA50, CA724, CA199, CEA, CA242, CK-BB, and HCG, significantly correlate, according to Pearson multiple correlation analyses ( $n = 73$  per parameter). **(H)** Pearson  $r$ : multiple linear regression showing the overall association between ZDHHC6 protein levels and other tumor markers, such as CK-BB, HCG, CEA, CA242, CA724, CA199, CA125, and CA50 ( $n = 73$  per parameter) Data are expressed as mean  $\pm$  SEM. The relevant experiments presented in this part were performed independently at least three times.  $P < 0.05$  indicates statistical significance

in human CRC cell lines was significantly decreased in a dose-dependent manner when exposed to a concentration gradient of 2-BP, as shown in Fig. 2F and G. In addition, the administration of 2-BP leads to the inhibition of ZDHHC6, which is directly associated with the decrease in Ki67-positive colon cancer cells. This correlation is supported by the results of an in vitro immunofluorescence experiment (Fig. 2H).

Considering the significant impact of ZDHHC6 on the advancement of colorectal cancer (CRC) and its probable involvement in the metabolic processes of tumours, we further examined the influence of ZDHHC6 on the molecular metabolism of CRC. To characterise the disrupted metabolic processes in colorectal cancer (CRC), a high-throughput metabolomics analysis was conducted to identify the metabolites that were significantly altered in 10 sets of CRC and adjacent normal tissues (Fig. 3A, B). In comparison to the adjacent normal tissues, there are 39 metabolites that exhibit significant changes in the cancerous tissues. The elevated metabolites consist primarily of lipids and lipid-like compounds, specifically fatty acids (FAs), phosphatidylcholine (PC), phosphatidylethanolamine (PE), lysophosphatidylethanolamine (LPE), sphingomyelin (SM), and lysophosphatidylcholine (LPC) (Fig. 3C). An additional analysis was conducted to determine the enrichment of specific pathways utilising 39 metabolites that showed differential expression. The results indicated that the production of triacylglycerol, glycerol phosphate shuttle, and palmitoylated protein were enriched (Fig. 3D, E). The findings validated that the lipidome composition exhibited a substantial increase in CRC tissues. However, the potential explanation for this abnormally vigorous lipid metabolism in CRC tissues remains uncertain. To investigate the potential connection between the abnormally increased lipidome in CRC and the expression of ZDHHCs, we analysed the expression of ZDHHCs in the aforementioned pairings of cancerous and neighbouring normal tissues. Our findings revealed that ZDHHC6 was the ZDHHC member with the highest level of expression, as shown in Fig. 3F. The modified expression of ZDHHC6 was strongly associated

with the synthesis of lipids and lipid-like metabolites in SNU-C2A and HCT116 cells when ZDHHC6 was either suppressed (shZDHHC6) or enhanced (AdZDHHC6) (Supplementary Fig. 2C, D). The Pearson multiple correlation and multiple linear regression analyses revealed a significant association between the levels of ZDHHC6 protein and various tumour markers, including CA125, CA50, CA724, CA199, CEA, CA242, CK-BB, and HCG (Fig. 3G, H). These findings indicate a potential correlation between elevated levels of ZDHHC6 and an aberrant rise in lipid and lipid-like metabolites in CRC. However, the precise function of ZDHHC6 in lipid metabolism in CRC remains uncertain.

#### ZDHHC6 enhances lipid deposition and carcinogenesis in CRC cells

Consistent with our previous findings, we conducted additional experiments to specifically determine the function of ZDHHC6 in colorectal cancer (CRC). We investigated the impact of introducing AdZDHHC6 or AdshZDHHC6 into SNU-C2A and HCT116 cells on their rate of cell division (Supplementary Fig. 3A, B). Interestingly, SNU-C2A and HCT116 cells that were transfected with AdshZDHHC6 showed a significant decrease in cell viability and EdU staining intensity. Conversely, cells transfected with AdZDHHC6 exhibited an increase in cell viability and EdU intensity. These findings suggest that alterations in ZDHHC6 expression in CRC cells may have an impact on proliferation in a laboratory setting (Supplementary Fig. 3C, D). Furthermore, our current study supports the notion that ZDHHC6 may play a role in the development of colorectal cancer (CRC) pathogenesis. This is consistent with our findings, as demonstrated by the transwell analysis, which showed a significant decrease in the invasion and migration of tumor cells when ZDHHC6 was silenced, compared to the control group (Supplementary Fig. 3E, F). Consistent with expectations, the levels of epithelial-mesenchymal transition (EMT)-related markers such as vimentin, N-cadherin, fibronectin, TGF $\beta$ 1, and MMP13 were significantly reduced in SNU-C2A and HCT116 cells. Conversely, the

expression of E-cadherin was greatly increased (Supplementary Fig. 3G, H). Furthermore, in vivo experiments demonstrated that inhibiting ZDHHC6 effectively decreased the rates of tumor growth and the weights of tumors in mice that had been implanted with the SNU-C2A tumor models (Supplementary Fig. 3I). The findings confirmed that the lack of ZDHHC6 played a role in inhibiting the growth of colon cancer cells and the process of EMT. Afterward, we discovered 36 metabolites that showed substantial changes in ZDHHC6-deletion CRC cells. Fatty acid metabolites exhibited a considerable drop in HCT116 cells lacking ZDHHC6. Furthermore, we conducted pathway enrichment analysis on the set of 36 metabolites and observed a significant association between ZDHHC6 and the pathways related to fatty acid production (Fig. 4A-C). Glucose is a crucial source for the creation of fatty acids through *de novo* biosynthesis. Subsequently, we employed glucose [ $U\text{-}^{13}\text{C}$ ] to monitor the process of fatty acid production. Our findings revealed that the cells with ZDHHC6 knockdown exhibited a substantial reduction in the labeling of palmitic acid and stearic acid from the glucose trackers (Fig. 4D, Supplementary Fig. 4A). In contrast, the HCT116 cells that had an enhanced expression of ZDHHC6 showed a considerable increase in the labeling of palmitic acid and stearic acid from glucose (Fig. 4E, Supplementary Fig. 4A). In addition, ZDHHC6 markedly enhanced the formation of triglycerides in HCT116 cells, as demonstrated by the bodipy staining experiment (Fig. 4F). Additionally, we conducted analogous tests on SW48, HT-29, and Caco-2 cell lines. We noted a substantial increase in the expression of several fatty acids and triglycerides in the colorectal cancer cells that were overexpressing ZDHHC6 (Supplementary Fig. 4B, C). Collectively, these findings offer proof that ZDHHC6 is crucial in the buildup of lipid content and may stimulate the production of fatty acids from scratch in CRC cells.

Subsequently, we conducted experiments involving both loss-of-function and gain-of-function assays on CRC cell lines to validate the involvement of ZDHHC6 in carcinogenesis. To investigate the role of ZDHHC6 in colorectal cancer (CRC) cells in living organisms, we implanted ZDHHC6-deficient HCT116 cells and ZDHHC6-overexpressing HCT116 cells under nude mice. Tumor sizes and weights were significantly reduced in animals implanted with ZDHHC6-deficient HCT116 cells compared to those implanted with control cells (Fig. 4G, H). In contrast, the upregulation of ZDHHC6 enhanced the tumorigenic capacity of HCT116 cells (Supplementary Fig. 4D). Conversely, the tumours originating from ZDHHC6-deleted HCT116 cells exhibited a notable reduction in several lipid metabolites, such as fatty acids, when compared to tumours formed from control cells (Fig. 4I). In summary, our data validate that

ZDHHC6 significantly contributes to lipid buildup and carcinogenesis in CRC.

#### ZDHHC6 specifically targets and interacts with lipid metabolism key transcription factor of PPAR $\gamma$

To explore the impact of ZDHHC6 on lipid accumulation in colorectal cancer (CRC), we conducted high-throughput RNA sequencing analysis to examine the possible effects of ZDHHC6 on key enzymes involved in fatty acid synthesis in CRC cells. Out of the top 36 genes that showed significant differences in expression, previously identified genes involved in the production of free fatty acids (FFA) were shown to be responsive to the depletion of ZDHHC6 (Supplementary Fig. 5A). The overexpression of ZDHHC6 was found to be linked to the process of lipid biosynthesis, as proven by GO-biological process analysis (Supplementary Fig. 6A). Subsequent GSEA analysis revealed that the gene sets related to the production of fatty acids were considerably increased in HCT116, Caco-2, SNU-C2A, and SW48 cells that were transduced with ZDHHC6 overexpression, as supported by Supplementary Fig. 6B. The abnormal increase in fatty acid synthesis is strongly associated with the main metabolic enzymes ACLY, ACC, FASN, and SCD1. To validate the role of ZDHHC6 in regulating fatty acid metabolic genes, we conducted qPCR analysis on CRC cells with ZDHHC6 knockdown and cells with ZDHHC6 overexpression. The mRNA levels of ACC, ACLY, FASN, and SCD1 were reduced in the ZDHHC6-knockdown HCT116 and SNU-C2A cells, but increased in the ZDHHC6-overexpressing cells (Supplementary Fig. 5B). In addition, we conducted a thorough investigation to determine the potential involvement of ZDHHC6 in the regulation of fatty acid degradation. To achieve this, we analyzed the expression of enzymes related to fatty acid degradation (ACOX-1, CPT1A, LCAD, UCP2, and MCAD) in stable cells engineered with ZDHHC6. We employed qRT-PCR and observed that ZDHHC6 indeed influenced the expression of these enzymes in CRC cells (Supplementary Fig. 6C-G). To verify the role of ZDHHC6 in promoting lipidome accumulation via ACC and ACLY, we introduced ZDHHC6 into HCT116 and SNU-C2A cells that had been depleted of ACC or ACLY. Our findings indicate that the introduction of ZDHHC6 did not significantly enhance the buildup of intracellular fatty acids and triglycerides in the ACC or ACLY knockdown cells, as observed in cells transfected with ZDHHC6 alone (Supplementary Fig. 5C, D). Collectively, these findings suggest that ZDHHC6 enhances the accumulation of lipid molecules by upregulating the expression of ACC and ACLY in colorectal cancer.

Subsequently, to determine the precise substrate targeted by ZDHHC6, which has the ability to control the production of ACC and ACLY, we employed a method

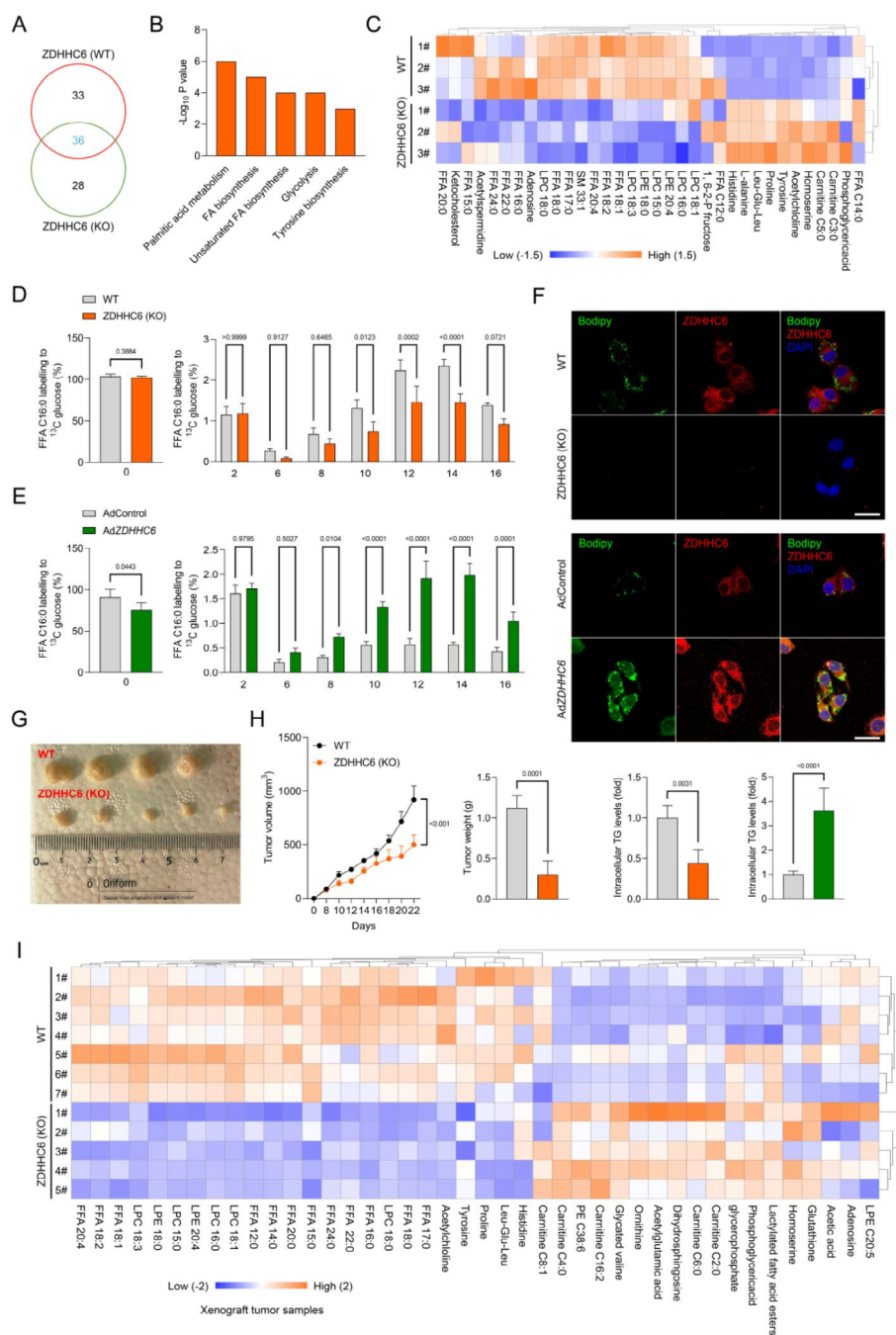


**Fig. 4** ZDHHC6 facilitates lipid deposition and carcinogenesis in CRC cells. **(A)** A Venn diagram shows the variations in metabolites produced by HCT116 cells with ZDHHC6 knockout (KO) and wild-type (WT) phenotypes. ZDHHC6 and fatty acid synthesis pathways have a significant association, according to pathway enrichment analysis of the 36 metabolites. Total peak area was used to correct the LC-MS-based untargeted metabolomic study and its findings. **(B)** Using these 36 differential metabolites, pathway analysis showed enhanced signaling pathways. ([www.metaboanalyst.ca](http://www.metaboanalyst.ca)). **(C)** A heatmap showing how these 36 significantly altered metabolites changed. Student's *t*-test, unpaired, two-tailed,  $P < 0.05$ . The fold change is indicated by  $-2.0 \sim 2.0$  (Fc). **(D, E)** The ratios of various isotopic forms of FFA C16:0 (palmitate) in ZDHHC6 (KO) (D) and AdZDHHC6 (E) HCT116 cells after a brief exposure to glucose [ $U\text{-}^{13}\text{C}$ ]. When the cell density was around 85%, the media was changed to RPMI 1640 containing 2 g/L glucose tagged with [ $U\text{-}^{13}\text{C}$ ]. Following a 24-hour period, the PBS-rinsed cell culture plates were quickly frozen in liquid nitrogen and subjected to an LC-MS assay analysis ( $n = 4$  per group). **(F)** Representative immunofluorescence pictures of HCT116 cells with ZDHHC6 (WT) and ZDHHC6 (KO) phenotypic, demonstrating ZDHHC6 expression, lipid accumulation (Bodipy staining), and corresponding intracellular triglyceride (TG) levels ( $n = 4$  per group). **(G, H)** ZDHHC6 (WT) and ZDHHC6 (KO) HCT116 cells were injected into the right flanks of nude mice. Every two days, tumor volumes were measured. On day 22 following dissection, tumor pictures (G), growth curves, and weight (H) were recorded ( $n = 4$  per group). Scale bars, 1 cm. **(I)** A heatmap utilizing untargeted metabolomic analysis comparing significantly changed metabolites between tumors originating from ZDHHC6 (KO) HCT116 cells and ZDHHC6 (WT) cell lines. Data are expressed as mean  $\pm$  SEM. The relevant experiments presented in this part were performed independently at least three times.  $P < 0.05$  indicates statistical significance

of isolating the ZDHHC6-associated protein complex in HCT116 cells using tandem affinity purification, followed by analysis using mass spectrometry. Notably, PPAR $\gamma$  (PPARG) was ranked at the top of the list (Fig. 5A). In addition, our research revealed that PPAR $\gamma$  is the sole counterpart among many transcription factors associated with lipid metabolism, such as PPAR $\alpha$ , PPAR $\delta$ , and SREBF1 (Fig. 5B). Furthermore, endogenous PPAR $\gamma$  was found in endogenous ZDHHC6 immunoprecipitates from SNU-C2A, SW48, HT-29, LS1034, and Caco-2 cells (Fig. 5C). Through in vitro pulldown tests using purified recombinant proteins, it was shown that ZDHHC6 directly interacts with PPAR $\gamma$ , as depicted in Fig. 5D. Given significant potential correlation of ZDHHC6 with PPAR $\gamma$ , we next integrated the ZDHHC6-interacting proteins obtained from the IP-MS experiment and the upregulated proteins revealed by proteomics analysis, and we identified PPAR $\gamma$  as the protein that interacts with and is regulated by ZDHHC6 using human HCT116, Caco-2, SNU-C2A and HT-29 colon cancer cell lines (Fig. 5E). Moreover, to further demonstrate the specific target of ZDHHC6 responsible for its specific function, we performed an additional immunoprecipitation-MS (IP-MS) analysis of Flag-ZDHHC6 and His-PPAR $\gamma$ -transfected HCT116, Caco-2, SNU-C2A, and HT-29, respectively, and identified 126 detectable potential ZDHHC6-interacting proteins. We then integrated the ZDHHC6-interacting proteins obtained from the IP-MS experiment and the upregulated proteins revealed by proteomics analysis, and we identified PPAR $\gamma$  as the key protein that interacts with and is regulated by ZDHHC6 (Fig. 5E). On the other hand, Flag-ZDHHC6 and His-PPAR $\gamma$  were overexpressed in HCT116, Caco-2, SNU-C2A, and HT-29, respectively. Co-immunoprecipitation (Co-IP) experiments demonstrated that ZDHHC6 co-immunoprecipitated with PPAR $\gamma$ , and vice versa (Fig. 5F). Glutathione *S*-transferase (GST) pull-down assay suggested that ZDHHC6 interacts directly with PPAR $\gamma$  in transfected Caco-2 and SNU-C2A cells, respectively (Fig. 5G). This GST pull-down result is consistent with the direct protein interaction of ZDHHC6 and PPAR $\gamma$  in HCT116 cells (Fig. 5D). The immunofluorescent staining test demonstrated a localization of ZDHHC6 (major in the cytoplasm) and PPAR $\gamma$  (major in the nucleus) mostly within the CRC cells (Fig. 5H). According to reports, PPAR $\gamma$  is composed of three distinct structural domains: AF-1, DBD, and the hinge region. Pull-down experiments demonstrated a robust association between ZDHHC6 and the DBD fragment of PPAR $\gamma$ , but only a few interactions were observed with the hinge-region fragment (Fig. 5I). In addition, an examination of the TCGA-CRC and ICGC-CRC databases revealed a substantial correlation between ZDHHC6 and the PPAR $\gamma$  pathway in CRC, as demonstrated in Fig. 5J. In summary, our findings validate that

ZDHHC6 has a unique interaction with PPAR $\gamma$ , a crucial transcription factor involved in lipid metabolism.

#### ZDHHC6 palmitoylates and stabilizes PPAR $\gamma$

Given the strong association between ZDHHC6 and PPAR $\gamma$ , as well as the crucial role of ZDHHC6 as a palmitoyltransferase in various biological processes, we hypothesized that ZDHHC6 may regulate the palmitoylation of PPAR $\gamma$  in response to alterations in lipid metabolism that occur during the progression of CRC. Therefore, to determine the role of palmitoylated PPAR $\gamma$  in the advancement of CRC, we analyzed its expression patterns and changes in response to 2-bromopalmitate (2-BP), a broad inhibitor of protein palmitoylation. Upon incubation of HCT116 cells with 2-BP to decrease the levels of palmitoylated proteins, there was a significant decrease in the expression of PPAR $\gamma$ , both in terms of protein abundance and pan-palmitoylation contents (Fig. 6A). In contrast, the expression levels of PPAR $\gamma$  in HCT116 cells were increased by the overexpression of palmitoylation by the use of palmostatin B (Palm B), palmostatin M (Palm M), or ABD957, which is an inhibitor of depalmitoylase enzymes. This increase in expression levels was confirmed through colocalization immunofluorescence analysis (Fig. 6A). In order to assess the impact of 2-BP on the decrease of PPAR $\gamma$  expression, a click chemistry assay was utilized to visualize the palmitoylated PPAR $\gamma$  (Fig. 6B). The presence of palmitoylation on PPAR $\gamma$  was verified using the streptavidin beads-mediated pulldown and western blotting analysis, as anticipated (Fig. 6B).

Furthermore, given the significant role of palmitoylation in the control of PPAR $\gamma$  stability, we were compelled to determine the precise position of palmitoylation on PPAR $\gamma$ . The function investigation involved determining the anticipated location of the palmitoylation site on PPAR $\gamma$  for *Homo sapiens* and *Mus musculus*. This was achieved through a combined analysis of the GPS-Palm software (MacOS\_20200219) developed by The CUCKOO Workgroup (<http://gpspalm.biocuckoo.cn/>) and the MDD-Palm algorithm (<http://csb.cse.yzu.edu.tw/MDDPalm/>). Both methods fortuitously anticipated and furnished the foremost 4 palmitoylation sites for PPAR $\gamma$ , exhibiting distinct confidence intervals and quality ratings. It is worth mentioning that cysteine 313 (C313) in human PPAR $\gamma$  and mouse PPAR $\gamma$  were identified as the most probable and dependable location for protein palmitoylation modification (Fig. 6C). Furthermore, the cysteine residue location exhibited significant conservation across many species taxa, as depicted in Fig. 6C. The presence of PPAR $\gamma$  protein in HCT116 and SNU-C2A cells was confirmed by detecting the residual PPAR $\gamma$  WT, C176S, C159S, C156S, and C313S mutants following CHX injection. As predicted, only the C313S

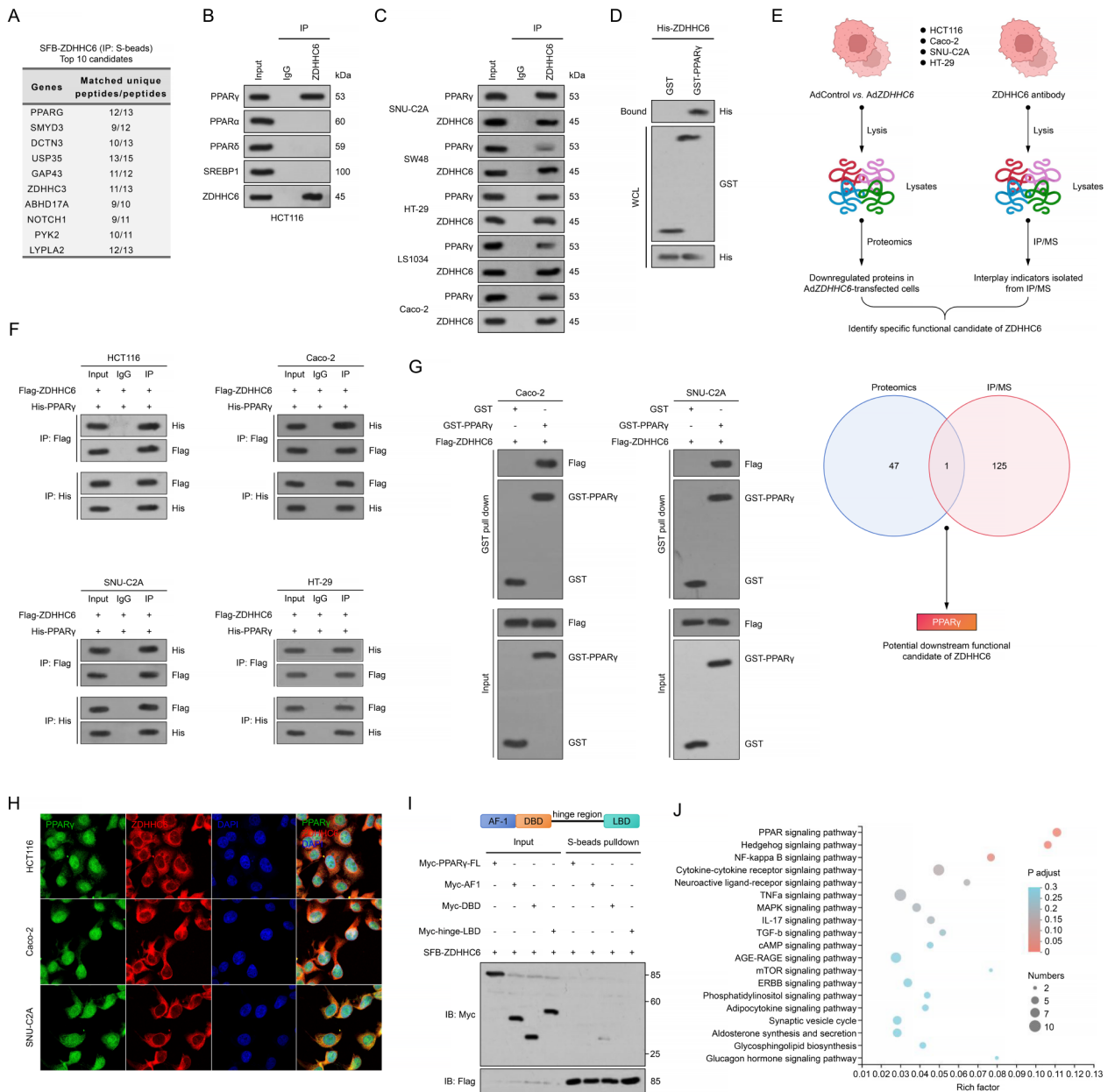


**Fig. 5** ZDHHC6 specifically binds to the lipid metabolism key transcription factor of PPAR $\gamma$ . **(A)** After 24 h of SFB-ZDHHC6 transfection in HCT116 cells, ZDHHC6-interacting proteins were identified by tandem affinity purification and mass spectrometry (MS). This was accomplished by removing S-protein, Flag, and streptavidin binding peptide (SFB). **(B)** ZDHHC6 or IgG antibodies were used to immunoprecipitate HCT116 cell lysates, and PPAR $\gamma$ , PPAR $\alpha$ , PPAR $\delta$ , SREBP1, and ZDHHC6 antibodies were used for western blotting experiments. **(C)** ZDHHC6 or IgG antibodies were used to immunoprecipitate cellular lysates of SNU-C2A, SW48, HT-29, LS1034, and Caco-2 cells, and ZDHHC6 or PPAR $\gamma$  antibodies were used for western blotting experiments. **(D)** GST pull-down assay using GST-PPAR $\gamma$  and purified His-ZDHHC6 in HCT116 cells. **(E)** Schematic of the experimental procedure showing the genes expression in HCT116, Caco-2, SNU-C2A and HT-29 after adenovirus-mediated *ZDHHC6* overactivation (*AdZDHHC6*). The lower schematic diagram showing the intersection of the results from the proteomics and IP-MS analyses. **(F)** For a duration of 24 h, plasmids expressing Flag-PPAR $\gamma$  or Myc-ZDHHC6 individually or in combination were transfected into HCT116, Caco-2, SNU-C2A and HT-29 cells, respectively. His or Flag antibodies were used for immunoblotting after cellular lysates had been immunoprecipitated with Flag and/or His antibodies. **(G)** GST pull-down assay using GST-PPAR $\gamma$  and purified Flag-ZDHHC6 in Caco-2 and SNU-C2A cells, respectively. **(H)** Assay for immunofluorescence staining demonstrating ZDHHC6 and PPAR $\gamma$  co-expression in HCT116, Caco-2, and SNU-C2A cells. 20  $\mu$ m. **(I)** In HCT116 cells, vectors containing the hinge-LBD domain, full length (FL), AF-1, DBD, and PPAR $\gamma$  were co-expressed with SFB-ZDHHC6. S-bead pulldown was used to immunoprecipitate cellular lysates. **(J)** Based on GSEA signaling pathway analysis, an assay of the TCGA-CRC and ICGC-CRC datasets showed a significant connection between ZDHHC6 and the PPAR $\gamma$  pathway in CRC. Data are expressed as mean  $\pm$  SEM. The relevant experiments presented in this part were performed independently at least three times.  $P < 0.05$  indicates statistical significance

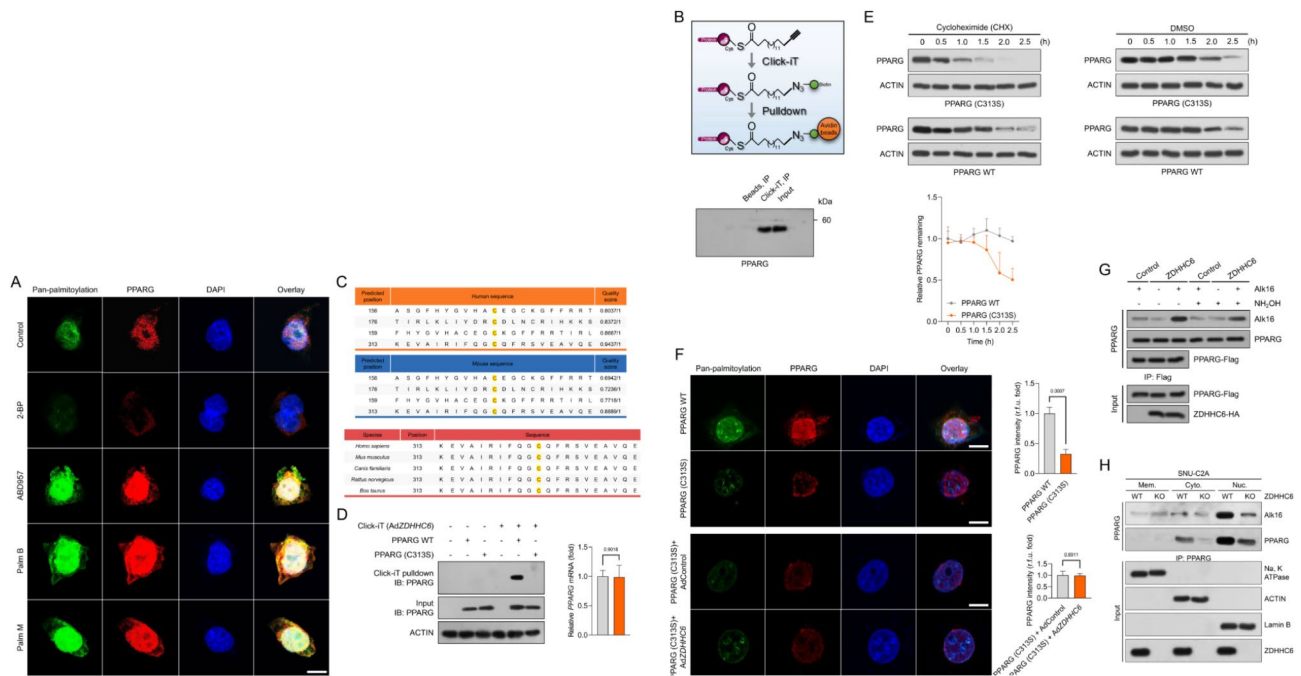


**Fig. 6** Identification of the palmitoylation site on PPAR $\gamma$  at evolutionarily conserved cysteine residues. **(A)** For a duration of 24 h, HCT116 cells were exposed to 60  $\mu$ M 2-BP, 1  $\mu$ M ABD957, 6  $\mu$ M palmostatin B (Palm B), and 10  $\mu$ M palmostatin M (Palm M) treatments. The slices that were fixed underwent immunofluorescence labeling using PPAR $\gamma$  (red) and pan-palmitoylation (green). 10  $\mu$ m scale bars;  $n=5$  per group. **(B)** Schematic diagram of the Click-iT assay for palmitoylation measurement of PPAR $\gamma$ . HCT116 cells were treated with 100  $\mu$ M Click-iT PA and azides for five hours. The resulting lysates were then submitted to Click-iT detection as per the product instructions, and PPAR $\gamma$  antibody western blotting analysis was performed. The indicated group's expression of PPAR $\gamma$  is indicated by the western blotting bands on the right. **(C)** Using the GPS-Palm program (MacOS\_20200219) (The CUCKOO Workgroup, <http://gpspalm.biocuckoo.cn/>) and the MDD-Palm algorithm (<http://csb.cse.yzu.edu.tw/MDDPalm/>), the palmitoylation site on PPAR $\gamma$  in Homo sapiens (upper) and Mus musculus (lower) is predicted to be located. PPAR $\gamma$ 's lower palmitoylation site contains conserved cysteine residues shared by *Rattus norvegicus*, *Bos taurus*, *Canis familiaris*, *Mus musculus*, and *Homo sapiens*. **(D)** After incubating Click-iT PA and azides for five hours on HCT116 cells overexpressing either PPAR $\gamma$  WT or PPAR $\gamma$  C313S mutant, the corresponding cellular lysates were obtained and Click-iT detection was performed in compliance with the product's instructions. After the palmitoylated proteins were added to the streptavidin-sepharose bead conjugate for pull-down detection, PPAR $\gamma$  and ACTIN antibodies were used in a western blotting examination. While PPAR $\gamma$  C313S was not palmitoylated in top gel, lane 6, or the control groups, it was for PPAR $\gamma$  WT in lane 5. Three separate runs of this experiment were conducted. **(E)** CHX was cultured with HCT116 cells overexpressing either the PPAR $\gamma$  WT or PPAR $\gamma$  C313S mutant for a specific amount of time. PPAR $\gamma$  and ACTIN antibodies were used in immunoblotting detection of the obtained cellular lysates. The relative PPAR $\gamma$  remaining ratio ( $n=4$  per group) is displayed in the right curve graph at the specified time point. **(F)** PPAR $\gamma$  WT or PPAR $\gamma$  C313S mutant overexpression was observed in the upper HCT116 cells. Pan-palmitoylation (green) and PPAR $\gamma$  (red) immunofluorescent labeling were applied to the cell sections. Lower, AdZDHHC6+PPAR $\gamma$  C313S mutant or PPAR $\gamma$  C313S alone were overexpressed in HCT116 cells, respectively. The bar graph displays the intensity of PPAR $\gamma$  fluorescence in each of the indicated groups ( $n=5$  pictures;  $P<0.05$  vs. PPAR $\gamma$  C313S+AdControl or PPAR $\gamma$  WT). Scale bars, 20  $\mu$ m. **(G)** In HCT116 cells, PPAR $\gamma$ -Flag and ZDHHC6-HA plasmids were transfected. Alk16 labeling was used to determine the palmitoylated PPAR $\gamma$  expression contents in the presence or absence of hydroxylamine therapy. **(H)** PPAR $\gamma$ -Flag was used to transfect SNU-C2A cells (WT) or ZDHHC6-deleted SNU-C2A cells, and Alk16 was used to label the cells. Subcellular fraction was extracted, and the levels of PPAR $\gamma$  protein were adjusted to verify that the input cells from the wild type and the knockout cell had the same quantity of PPAR $\gamma$ . Immunoblotting analysis was used to evaluate the palmitoylated PPAR $\gamma$  expression contents in the cell membrane (Mem.), cell cytoplasm (Cyto.), and cell nucleus (Nuc.) components. Data are expressed as mean  $\pm$  SEM. The relevant experiments presented in this part were performed independently at least three times.  $P<0.05$  indicates statistical significance

mutation showed a significant decrease in the amount of PPAR $\gamma$ , while the other variants did not show any significant changes (Supplementary Fig. 7A, B). The impact of a sequence of genetic alterations on the buildup of lipids in the specified transfected colorectal cancer (CRC) cells was additionally validated using immunofluorescence analysis (Supplementary Fig. 7C, D). Substitution of the C313 residue with serine completely inhibited the palmitoylation of PPAR $\gamma$ , as demonstrated by the Click-iT chemistry experiment (Fig. 6D). The C313S mutant significantly decreased the expression of PPAR $\gamma$  protein

profiles without affecting its mRNA levels (Fig. 6D). The PPAR $\gamma$  with C313S mutant underwent degradation in parallel with CHX treatment, leading to a progressive reduction in the remaining PPAR $\gamma$  levels (Fig. 6E), which was comparable to the impact of 2-BP administration. Considering the identification of C313 as the primary location for PPAR $\gamma$  palmitoylation, we are curious about the extent to which S-palmitoylation at C16 contributes to the chemical alteration of PPAR $\gamma$ . Hence, a sequence of alkyl-labeled fatty acids, namely Alk14, Alk16, Alk18, and Alk20, were employed to investigate this biological

phenomenon. PPAR $\gamma$  can be efficiently labeled with palmitoylation (using Alk16) but shows significantly lower efficiency when labeled with Alk14, stearoylation (Alk18), or Alk20 (Supplementary Fig. 8A-C). This suggests that C16-captured *S*-palmitoylation is the primary acyl group involved in the chemical alteration of PPAR $\gamma$ . Having the C313 mutation as the critical site of PPAR $\gamma$  palmitoylation, we next evaluated the functional impact of these mutants on C16-captured *S*-palmitoylation over the duration of alkynyl palmitic acid (Alk16) therapy. In the CRC cells that were genetically modified, the presence of PPAR $\gamma$  with human C313S effectively eliminated the labeling of palmitoylation (with Alk16). This was confirmed by the streptavidin pull-down study, which showed that C313 was necessary for the *S*-palmitoylation of the PPAR $\gamma$  protein (Supplementary Fig. 8A-C). Furthermore, the role of ZDHHC6 as the primary target for PPAR $\gamma$  was established using a comparative study. This analysis demonstrated the anticipated changes in the quantity of PPAR $\gamma$  protein in HCT116 cells when ZDHHC6 was overexpressed using adenovirus, both with and without the PPAR $\gamma$  C313S mutation. This was confirmed by an immunofluorescence assay (Fig. 6F). In addition, the absence of palmitoylation due to the C313S mutation resulted in a reduction in the simultaneous expression of PPAR $\gamma$  and pan-palmitoylation, as indicated in Fig. 6F. Based on our previous findings, we have determined the interaction between ZDHHCs and their targeted substrates. The Co-IP test clearly showed a strong direct binding between ZDHHC6 and PPAR $\gamma$  in the ectopic expression of CRC cells (Fig. 5). To enhance the visual representation of PPAR $\gamma$  palmitoylation in the presence of ZDHHC6, we employed Alk16 as a metabolic marker to assess the impact of ZDHHC6 on palmitoylated PPAR $\gamma$  and its movement inside cells, similar to what was shown in Supplementary Fig. 8. The presence of NH<sub>2</sub>OH significantly reduced the levels of palmitoylation on PPAR $\gamma$ , suggesting that the increase in palmitoylated PPAR $\gamma$  primarily occurred on cysteine residues and was caused by the action of ZDHHC6 (Fig. 6G). Analysis of fractionation in ZDHHC6 wild-type or ZDHHC6-deficient HCT116 cells indicated that the palmitoylation of PPAR $\gamma$  by ZDHHC6 increased the quantity of the modified PPAR $\gamma$  protein specifically in the cell nucleus, but not in other cellular components (Fig. 6H). The reliable outcomes of modifying the level of PPAR $\gamma$  through palmitoylation were further validated in HCT116 cells that overexpressed ZDHHC6 (Supplementary Fig. 8D). The aforementioned results consistently demonstrated that ZDHHC6 plays a crucial role as a primary palmitoyltransferase in the formation of palmitoylated PPAR $\gamma$ . Furthermore, its function exhibited a significant correlation with the advancement of colorectal cancer in human individuals.

#### **Upregulated ZDHHC6-mediated palmitoylated PPAR $\gamma$ promotes its nucleus translocation**

Following the identification of ZDHHC6 as the primary palmitoyltransferase for PPAR $\gamma$ , the subsequent step was examining the impact of ZDHHC6 on the nucleus localization of PPAR $\gamma$ . This enzyme had an impact not only on the stabilization of PPAR $\gamma$  throughout the process of ZDHHC6 knockdown, but also on the palmitoylation of PPAR $\gamma$  (Fig. 7A-C). In addition, the expression of ZDHHC6 by ectopic expression in HCT116, SNU-C2A, SW48, HT-29, and Caco-2 cells led to an increase in the expression of PPAR $\gamma$  protein and a speeding up of its translocation to the nucleus of the CRC cells (Fig. 7D, E). The purpose of this investigation was to determine whether ZDHHC6 interacts with PPAR $\gamma$  in additional colorectal cancer cells. This was done in consideration of the determination of the interaction between DHHCs and their targeted substrates. As a matter of fact, the Co-IP test demonstrated that the direct interaction between ZDHHC6 and PPAR $\gamma$  could be wonderfully observed in the ectopic expression of human Caco-2 cells (Fig. 7F). Furthermore, considering the fact that C313 site has been identified as the primary location for palmitoylation of PPAR $\gamma$ , we pose the question of whether or not the *S*-palmitoylation that was captured by C16 was the primary contributor to the chemical change of PPAR $\gamma$ . Consequently, to investigate this biological process, a series of alkyl-labeled fatty acylation operations, which included alk-C14, alk-C16, alk-C18, and alk-C20, were utilized. Palmitoylation (alk-C16) labels are able to successfully mark the PPAR $\gamma$ , whereas labels with alk-C14 chain lengths, stearoylation (alk-C18), or alk-C20 labels are significantly less effective in marking the PPAR $\gamma$  (Fig. 7G, H). The findings of this study suggest that the primary acyl group responsible for the chemical alteration of PPAR $\gamma$  is C16-captured *S*-palmitoylation. After determining that the C313S site mutation is the most important location for PPAR $\gamma$  palmitoylation, we proceeded to investigate the functional effects of these mutations on C16-captured *S*-palmitoylation during the course of treatment with alkynyl palmitic acid (alk-C16). It was anticipated that PPAR $\gamma$  with a human C313S site mutation would drastically eliminate palmitoylation (alk-C16) labels, as corroborated by streptavidin pull-down analysis, which further demonstrated that human C313S was necessary for *S*-palmitoylation of PPAR $\gamma$  protein (Fig. 7I). Moreover, to further visualize PPAR $\gamma$  palmitoylation in the presence of ZDHHC6, we utilized alk-C16 as a metabolic sign to investigate the effects of ZDHHC6 on palmitoylated PPAR $\gamma$  and its nucleus translocation. This was done in a manner that was comparable to the methodology described above. Incubation with NH<sub>2</sub>OH resulted in a significant reduction of palmitoylation levels on PPAR $\gamma$ , which suggests that the

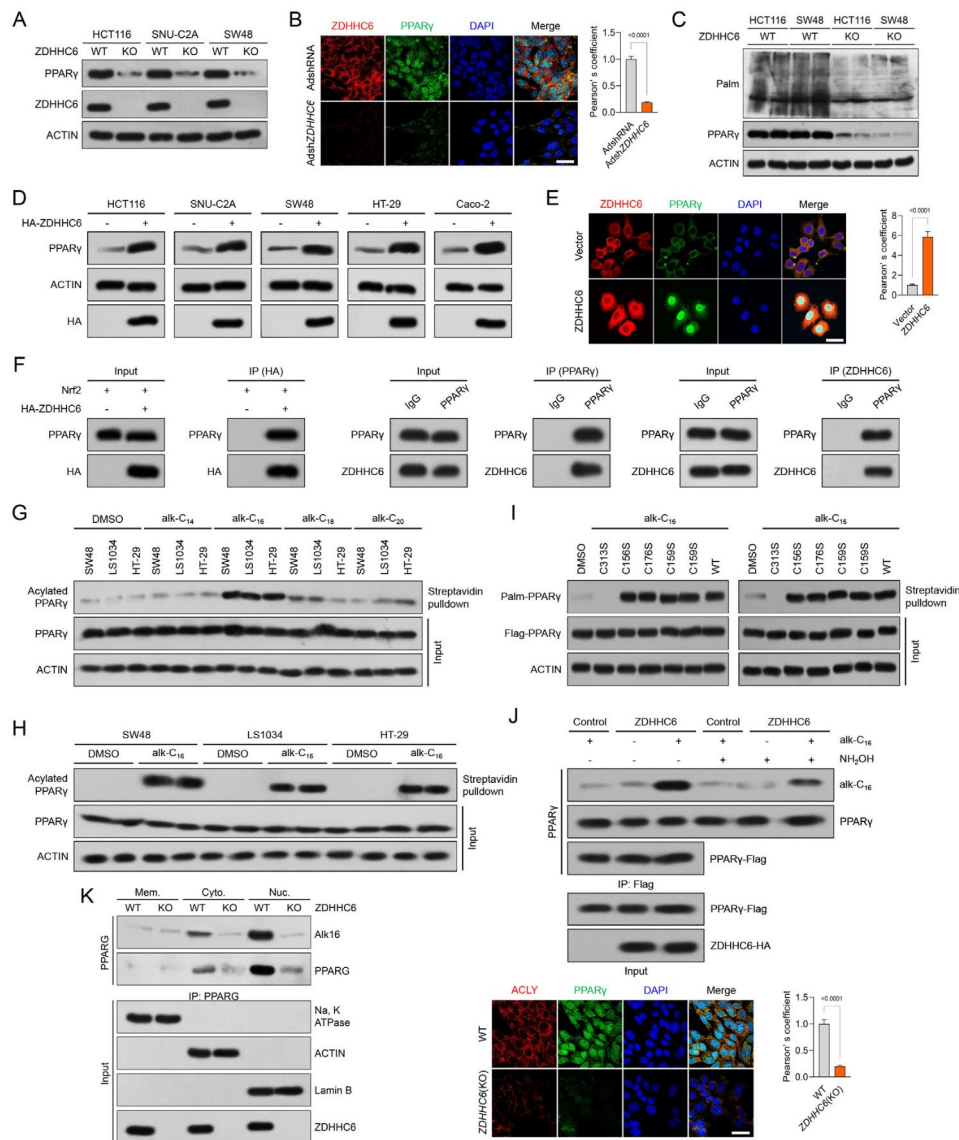


**Fig. 7** ZDHHC6-mediated palmitoylated PPAR $\gamma$  enhances its nucleus translocation. **(A)** ZDHHC6 and PPAR $\gamma$  expression were examined in the *ZDHHC6*-deleted HCT116, SNU-C2A and SW48 cells, respectively ( $n = 3$  per group). **(B)** ZDHHC6 and PPAR $\gamma$  co-expression in AdshZDHHC6-transfected HCT116 cells, along with the matching fluorescence density as determined by Pearson's analysis ( $n = 4$  per group;  $P < 0.05$  vs. AdshRNA). The scale bars are 20  $\mu\text{m}$ . **(C)** In *ZDHHC6*-deleted HCT116 or *ZDHHC6*-deleted SW48 cells, palmitoylation levels and PPAR $\gamma$  expression were analyzed using western blotting assay ( $n = 4$  per group). **(D)** Western blotting assay using PPAR $\gamma$ , ACTIN, and HA antibodies, followed by PPAR $\gamma$  overexpressing the HA-tagged ZDHHC6 construct in various CRC cell lines ( $n = 3$  per group). **(E)** Immunofluorescence pictures demonstrating the co-expression of PPAR $\gamma$  and ZDHHC6 in ZDHHC6-overexpressed HCT116 cells, together with the matching fluorescence density as determined by Pearson's analysis ( $n = 4$  per group;  $P < 0.05$  compared to empty vector). The scale bars are 20  $\mu\text{m}$ . **(F)** HCT116 cells underwent IP of HA after co-transfecting with PPAR $\gamma$  and HA-ZDHHC6. ZDHHC6 and PPAR $\gamma$  Mutual Co-IP shows that endogenous ZDHHC6 and PPAR $\gamma$  bind to each other in HCT116 cells. **(G)** Using various alkyl-labeled fatty acylation, such as alk-C<sub>14</sub>, alk-C<sub>16</sub>, alk-C<sub>18</sub>, and alk-C<sub>20</sub>, the palmitoylation of PPAR $\gamma$  in the indicated cells was detected. By using streptavidin bead pull-down to identify acylated PPAR $\gamma$ , an immunoblotting experiment using PPAR $\gamma$  and ACTIN antibodies ( $n = 6$  per group) was performed. **(H)** To identify acylated PPAR $\gamma$  in SW48, LS1034, and HT-29 cells, the same methodology as in (G) was applied. Following that, the lysates ( $n = 6$  per group) were subjected to western blotting analysis using PPAR $\gamma$  and ACTIN antibodies. **(I)** Using Click reaction-associated streptavidin pull-down, the palmitoylation levels of Flag-labeled PPAR $\gamma$  WT, PPAR $\gamma$  C313S, PPAR $\gamma$  C156S, PPAR $\gamma$  C176S, and PPAR $\gamma$  C159S mutants were examined. Three individuals per group underwent an immunoblotting experiment using Flag and ACTIN antibodies on the relevant lysates. **(J)** ZDHHC6-HA and PPAR $\gamma$ -Flag were the vectors used to transfect the HCT116 cells. Using alk-C<sub>16</sub> labeling, higher, palmitoylated PPAR $\gamma$  levels were demonstrated in both the presence and absence of hydroxylamine therapy. The corresponding fluorescence density and ACLY and PPAR $\gamma$  co-expression in HCT116 WT or HCT116 ZDHHC6 (KO) cells are depicted in the lower representative immunofluorescence images, which were analyzed using Pearson's method ( $n = 5$  per group;  $P < 0.05$  vs. WT). The scale bars are 20  $\mu\text{m}$ . **(K)** After transfecting the HCT116 WT or HCT116 ZDHHC6 (KO) cells with PPAR $\gamma$ -Flag, the cells were labeled with alk-C<sub>16</sub>. To verify that the wild type and knockout cell components for input had the same quantity of PPAR $\gamma$ , subcellular fraction was obtained and PPAR $\gamma$  protein levels were adjusted. Western blotting analysis was used to assess palmitoylated PPAR $\gamma$  levels in the cell membrane (Mem.), cell cytoplasm (Cyto.), and cell nucleus (Nuc.) components. Data are expressed as mean  $\pm$  SEM. The relevant experiments presented in this part were performed independently at least three times.  $P < 0.05$  indicates statistical significance

upregulation of palmitoylated PPAR $\gamma$  mostly happened on cysteine and was driven by ZDHHC6 (Fig. 7J). An additional protocol was made by fractionation analysis in ZDHHC6 wild-type or *ZDHHC6*-deficient Caco-2 cells, which indicated that ZDHHC6-mediated palmitoylation of PPAR $\gamma$  increased the quantity of the modified PPAR $\gamma$  protein in the nucleus, but not in the membrane or cytoplasm components (Fig. 7K). The studies presented above unambiguously demonstrated that ZDHHC6 is a significant palmitoyltransferase that plays a role in the occurrence of palmitoylated PPAR $\gamma$ , and the activity of this enzyme was found to have a favorable correlation with the progression of colorectal cancer.

#### **Palmitoylation-stabilized PPAR $\gamma$ suppresses its lysosome degradation**

Prior report has demonstrated that the significant rise in PPAR $\gamma$  protein levels effectively halted the process of lysosome degradation in the face of prolonged metabolic challenges and stress [36]. PPAR $\gamma$  is believed to undergo many posttranslational modifications that interact either positively or negatively to influence its protein destiny during different physiological and pathological states [36, 37]. Therefore, we examined the impact of palmitoylated PPAR $\gamma$  on the evolution of its breakdown in the lysosome. The rapid breakdown of the palmitoylation-deficient mutant PPAR $\gamma$  C313S and the buildup of cellular lipids could be reversed by the lysosomal inhibitors NH $_4$ Cl and Pepstatin A (Pep A), but not by the proteasomal inhibitor MG132 or the autophagy inhibitor 3-Methyladenine (3-MA) (Fig. 8A). In order to validate the lysosome-dependent mechanism, we utilized 2-BP to hinder the palmitoylation of naturally occurring PPAR $\gamma$  in HCT116 cells (Fig. 8B). Pep A and NH $_4$ Cl, but not 3-MA or MG132, were able to enhance the stability of PPAR following depalmitoylation and a decrease in destabilized PPAR $\gamma$ -related lipid accumulation (Fig. 8C, D).

PPAR $\gamma$ , a nuclear receptor, has been found to have a significant impact on glucose metabolism and overall energy balance through its posttranslational alterations [38]. Upon transportation to the cell nucleus, PPAR $\gamma$  can undergo various modifications such as phosphorylation, ubiquitination, and acetylation [39, 40]. These modifications can affect its activity, stability, and interaction with other molecules. Additionally, PPAR $\gamma$  may be internalized into recycle endosomes or degraded through the late endosome-lysosome pathway [41]. To investigate the impact of (de)palmitoylation on the movement of PPAR $\gamma$ , we inhibited the palmitoylation process of PPAR $\gamma$  and examined its distribution across various subcellular compartments. Consistent with expectations, the use of 2-BP significantly reduced the overlap of PPAR $\gamma$  with recycling endosomes indicated by Rab11, while increasing

its overlap with lysosomes labeled by Lamp1 and late endosomes labeled by Rab7b (Fig. 8E-G). The results consistently showed that depalmitoylation facilitated the degradation of PPAR $\gamma$  through the lysosomal pathway.

#### **ZDHHC6-mediated fatty acid biosynthesis promotes CRC carcinogenesis by upregulating PPAR $\gamma$**

To ascertain the impact of increased production of fatty acids on cell proliferation, we manipulated the expression of PPAR $\gamma$  in cells that either had ectopically produced PPAR $\gamma$  or had been subjected to *ZDHHC6*-knockdown. In our study, we examined the process of glucose oxidation converting into fatty acid synthesis. We accomplished this by cultivating cells with glucose that was consistently enriched with carbon-13 ([U- $^{13}$ C] glucose). We specifically focused on cells that had reduced levels of PPAR $\gamma$  and overexpressed ZDHHC6. Our findings showed that when ZDHHC6 was overexpressed alone, it greatly enhanced the labeling of fatty acids from glucose tracers. However, when ZDHHC6 was overexpressed along with the co-transfection of shPPAR $\gamma$ , the knockdown of PPAR $\gamma$  significantly reduced the labeling of fatty acids from glucose tracers (Fig. 9A). In contrast, the introduction of PPAR $\gamma$ -transduction greatly enhanced the process of labeling fatty acids from glucose tracers in HCT116 cells with ZDHHC6 knockdown (Fig. 9B). Furthermore, the analysis of bodipy green staining and PPAR $\gamma$  co-expression revealed a consistent pattern of lipid buildup in the aforementioned CRC cells (Fig. 9C, D). To further investigate the relationship between PPAR $\gamma$  and ZDHHC6, we manipulated the expression of PPAR $\gamma$  in cells lacking ZDHHC6 or cells overexpressing ZDHHC6 by co-transfecting them with a mutant form of PPAR $\gamma$  (PPAR $\gamma$  C313S). We conducted an experiment where we cultured cells with consistently labeled [U- $^{13}$ C] glucose in two different types of cells: *ZDHHC6*-knockout HCT116 cells and cells with ZDHHC6 restoration and AdPPARG C313S mutant co-transfection. As expected, we observed glucose oxidation leading to fatty acid biosynthesis in both types of cells. However, when PPAR $\gamma$  C313S expression was present, it counteracted the increase in fatty acid synthesis regulated by ZDHHC6 and significantly reduced the labeling of fatty acids from glucose tracers (Supplementary Fig. 9A). In *ZDHHC6*-knockdown HCT116 cells, there is no significant detection of enhanced fatty acid labeling from glucose tracers when PPAR $\gamma$  C313S mutant-transduction is used (Supplementary Fig. 9B). Furthermore, the immunofluorescence assay revealed a consistent pattern of lipid accumulation in the aforementioned CRC cells, as demonstrated by the co-expression of PPAR $\gamma$  and the bodipy green staining (Supplementary Fig. 9C, D). These findings indicate that ZDHHC6 enhances the production of fatty acids by stabilizing PPAR $\gamma$ . To additionally confirm the

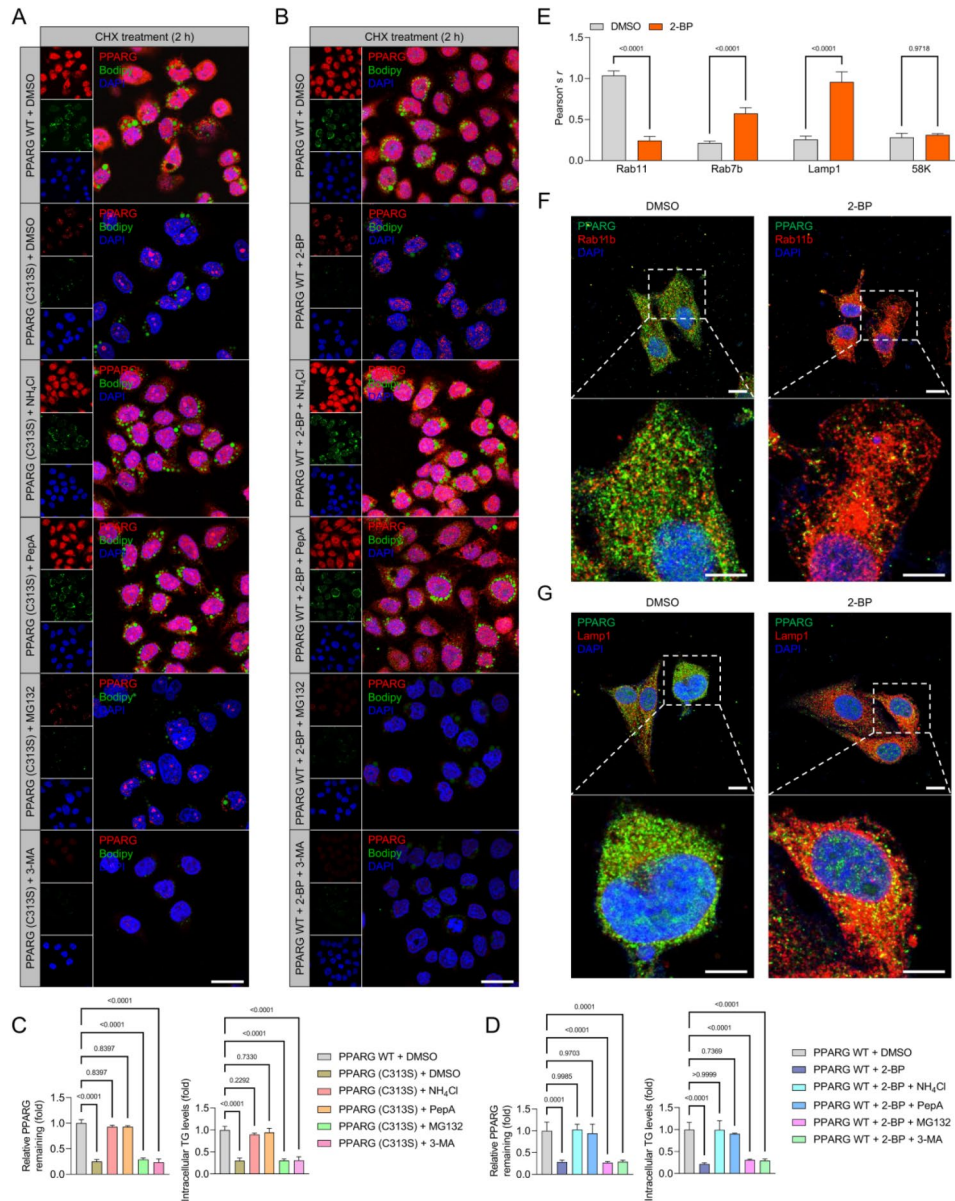


**Fig. 8** Palmitoylation obscures an inherent lysosomal sorting signalling in PPAR $\gamma$ . **(A)** Using immunofluorescence analysis through CHX-chase studies in the presence of lysosome inhibitors such as NH<sub>4</sub>Cl and Pepstatin A (PepA), autophagy inhibitor (3-MA), and proteasome inhibitor (MG132), the degradation and residual amount of PPAR $\gamma$  or the PPAR $\gamma$  C313S mutant in HCT116 cells was assessed.  $n=5$  per group. The scale bars are 20  $\mu$ m. **(B)** Immunofluorescence analysis demonstrating the intensity quantification based on the remaining relative level of PPAR $\gamma$ . Three separate independent runs of this experiment produced findings that were comparable.  $n=5$  per group. Scale bars: 20  $\mu$ m. **(C)** In HCT116 cells, the effects of lysosome inhibitor, autophagy inhibitor, and proteasome inhibitor were measured to evaluate the intracellular TG contents and relative levels of PPAR $\gamma$  remaining after (A).  $P < 0.05$  compared to WT;  $n=5$  per group. **(D)** In HCT116 cells, the relative amounts of residual PPAR $\gamma$  and the intracellular TG contents associated with (B) were measured.  $P < 0.05$  compared to WT;  $n=5$  per group. **(E)** The colocalization of PPAR $\gamma$  with Rab11, Rab7b, Lamp1, and 58 K in HCT116 cells treated with 2-BP or DMSO control was statistically determined.  $P < 0.05$  compared to DMSO;  $n=5$  per group. **(F)** Typical immunofluorescence pictures demonstrating the colocalization of endosome recycling marker Rab11b and ectopically produced PPAR $\gamma$  in HCT116 cells after a 2-BP challenge. Each group has  $n=5$  per group. Scale bars: 10  $\mu$ m. **(G)** Typical immunofluorescence pictures demonstrating the colocalization of lysosome marker Lamp1 and ectopically produced PPAR $\gamma$  in HCT116 cells during 2-BP stimulation. Each group has  $n=5$  per group. Scale bars: 10  $\mu$ m. Data are expressed as mean  $\pm$  SEM. The relevant experiments presented in this part were performed independently at least three times.  $P < 0.05$  indicates statistical significance

role of ZDHHC6 in promoting tumor formation through the activation of fatty acid production, we performed xenograft tumor tests utilizing the aforementioned cell lines. Significantly, mice that received implantation of

ZDHHC6-overexpressing HCT116 cells developed larger tumors in comparison to those implanted with control HCT116 cells. However, HCT116 cells that were simultaneously overexpressed with ZDHHC6 and co-transfected

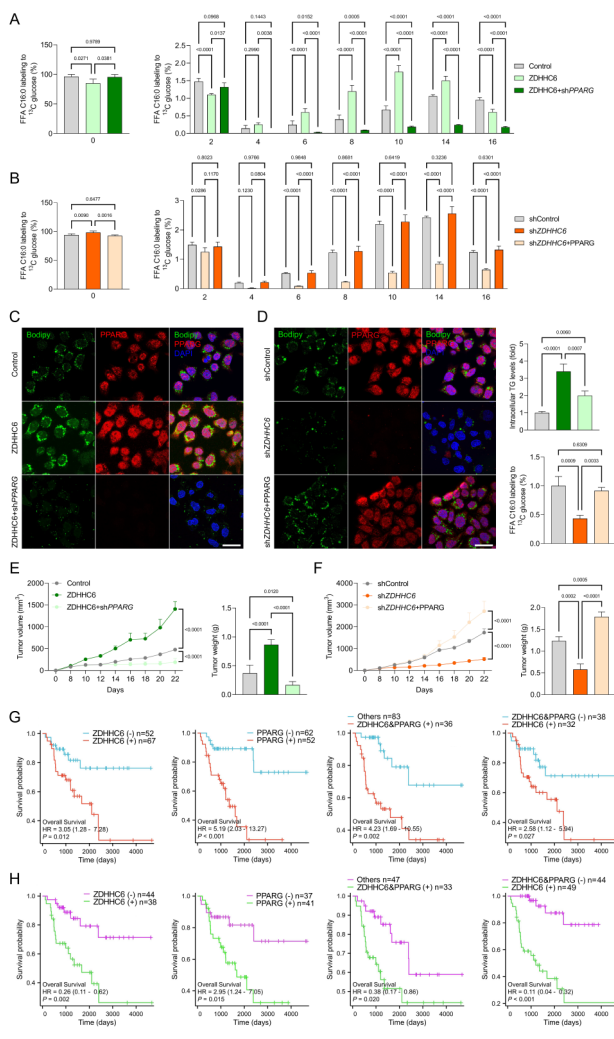


**Fig. 9** ZDHHC6-driven lipid biosynthesis contributes to CRC carcinogenesis by upregulating PPAR $\gamma$ . (A, B) In HCT116-related stable cells (Control, ZDHHC6, and ZDHHC6+shPPAR $\gamma$ ) (A) and HCT116-related stable cells (shControl, shZDHHC6, and shZDHHC6+PPAR $\gamma$ ) (B), the percentages of different isotopomers of FFA C16:0 following exposure to [U-<sup>13</sup>C] glucose are shown. Each group has  $n=5$ . (C, D) The relative TG content and PPAR $\gamma$  expression abundance in the aforementioned cell lines from (A) and (B) are displayed in representative immunofluorescence pictures. Each group has  $n=5$ . The scale bars are 20  $\mu$ m. (E) In null mice, right flanks were injected with ZDHHC6+shPPAR $\gamma$ , ZDHHC6, and Control, stable cells related to HCT116. Every two days, tumor volumes were measured. Weight and tumor growth curves were measured 22 days following dissection. Each group has  $n=5$ . (F) The right flanks of null mice were injected with shControl, shZDHHC6, and shZDHHC6+PPAR $\gamma$ , stable cells linked to HCT116. Every two days, tumor volumes were measured. Weight and tumor growth curves were measured 22 days following dissection. Each group has  $n=5$ . (G) Kaplan-Meier curves representing the survival analysis based on TCGA CRC prognostic data for ZDHHC6-positive, PPAR $\gamma$ -positive, and ZDHHC6 & PPAR $\gamma$  co-positive patients. (H) Based on the prognosis information from the ICGC CRC database, Kaplan-Meier curves were used to analyze the survival of ZDHHC6-positive, PPAR $\gamma$ -positive, and ZDHHC6 & PPAR $\gamma$  co-positive patients. Data are expressed as mean  $\pm$  SEM. The relevant experiments presented in this part were performed independently at least three times.  $P < 0.05$  indicates statistical significance

with shPPAR $\gamma$  or PPAR $\gamma$  C313S mutants exhibited lower rates of tumor growth (Fig. 9E; Supplementary Fig. 9E). In addition, mice that had been implanted with HCT116 cells in which ZDHHC6 had been suppressed and PPAR had been overexpressed exhibited higher rates of tumor formation compared to the CRC cells that had only been transfected with shZDHHC6 (Fig. 9F). In addition, the mice carrying the ZDHHC6 knockdown and mutant PPAR $\gamma$  C313S HCT116 cells exhibited significantly suppressed tumor formation compared to the mice with shControl (Supplementary Fig. 9F). The results demonstrate that increased expression of ZDHHC6 can stimulate the production of fatty acids in living organisms by activating PPAR $\gamma$ , hence promoting the advancement of colorectal cancer.

On top of that, we have found a strong positive correlation between ZDHHC6 and PPAR $\gamma$ , PPAR $\gamma$  and ALCY, and PPAR $\gamma$  and ACC transcript levels in the ICGC CRC and TCGA CRC databases. This correlation confirms the relationship between PPAR $\gamma$  and its associated factors during CRC formation (Fig. 1 and Supplementary Fig. 5). Subsequently, we assessed the predictive significance of ZDHHC6 and PPAR $\gamma$  in these datasets of colorectal cancer tissue microarrays (TMA). It is worth mentioning that patients with elevated levels of ZDHHC6 or PPAR $\gamma$  experienced significantly shorter overall survival compared to patients with low levels of ZDHHC6 or PPAR $\gamma$  in the TCGA CRC and ICGC CRC databases (Fig. 9G, H). To better understand the impact of PPAR $\gamma$  on the prognosis of ZDHHC6-positive CRC patients, we conducted an analysis of the prognostic value of ZDHHC6 in four different CRC databases: CGWB, UCSC, CANEVOLVE, and COSMIC. This analysis included a total of 671 patients, with those who died within 5 months or were followed up for less than 3 months being excluded. Additionally, we examined the correlation between ZDHHC6 and various factors such as pathologic state (I–IV), race, gender, and age in the indicated CRC datasets (Supplementary Fig. 9G–K). CRC patients exhibiting a single elevated level of ZDHHC6 demonstrated an unfavorable prognosis. Also, individuals with elevated levels of ZDHHC6 have poorer overall survival compared to those with lower levels of this factor. Furthermore, there is a positive association between ZDHHC6 levels and pathological state but no significant correlation with race, age, or gender. Together, we discovered a previously unknown harmful connection between ZDHHC6 and the variables that regulate the production of fatty acids and the balance of lipid oxidation, specifically related to PPAR $\gamma$ , in patients with colorectal cancer.

### Discussion

Disruption of cellular metabolism is a characteristic feature of the advancement of cancer. Alongside increased glycolysis, there are often abnormalities in fatty acid production and lipid oxidation in developing tumors, which are necessary to fulfill their metabolic needs [42, 43]. Fatty acid production is less active in quiescent cells, which primarily take up lipids from the extracellular circulation. On the other hand, *de novo* lipogenesis (DNL), particularly the production of new fatty acids, plays a significant role in providing tumor cells with a source of lipids [44]. In this study, we have discovered that ZDHHC6 functions as a palmitoyltransferase enzyme that controls the production of fatty acids. Specifically, ZDHHC6 directly adds palmitoyl groups to PPAR $\gamma$ , a protein involved in regulating gene expression. This palmitoylation process stabilizes PPAR $\gamma$ , leading to the activation of ACLY expression and the subsequent development of lipid buildup-related carcinogenesis (Fig. 10).

Alteration of the equilibrium in lipid oxidation and lipid synthesis is becoming a more significant contributor

to the development of colorectal cancer (CRC) [45]. This highlights the intricate relationship between cancer metabolism and cellular signaling pathways. The upregulation of enzymes like ACLY is responsible for this metabolic change, which not only supplies essential lipids for the formation of cell membranes but also enhances cancer-causing signaling pathways involved in cell survival, growth, and specialization [46, 47]. Moreover, the production of particular lipid species can influence the activation of these pathways, so strengthening a cancer-promoting milieu. Elevated fatty acid synthesis also affects cellular energy production and can modify the tumor microenvironment, so promoting a favorable setting for cancer advancement and spread. Inhibiting this process of lipid production has demonstrated encouraging outcomes in impeding tumor growth and is a tempting target for therapeutic intervention [48, 49]. Unraveling the exact ways in which fatty acid production and signaling pathways come together could reveal new possibilities for focused treatments in managing CRC [50]. The latest findings align with prior studies, although

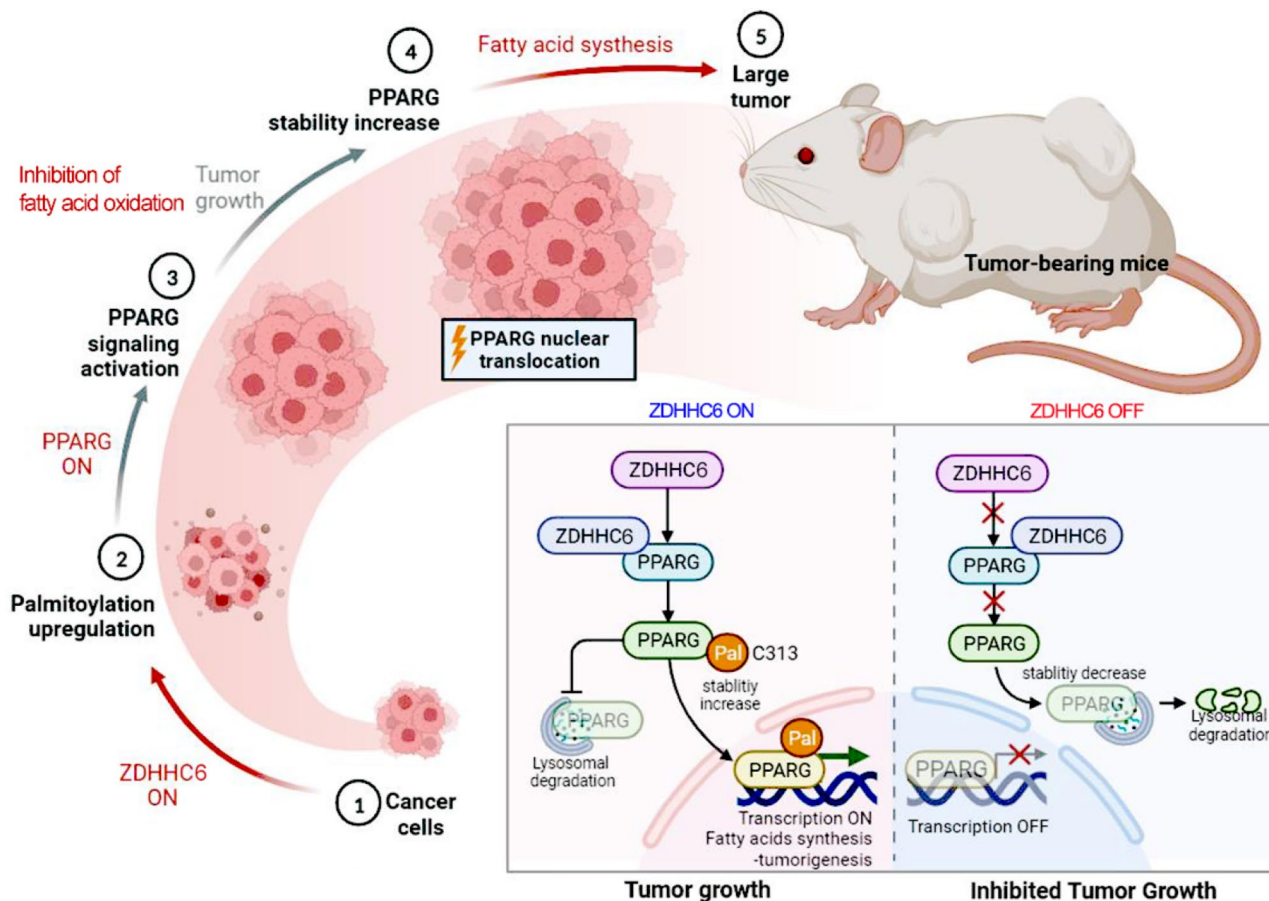


**Fig. 10** Palmitoylation stabilizes PPAR $\gamma$  by ZDHHC6 via blocking its lysosomal degradation to promotes lipid biosynthesis-associated CRC development. As a palmitoyltransferase enzyme, ZDHHC6 regulates the synthesis of fatty acids. To be more precise, ZDHHC6 directly attaches palmitoyl groups to PPAR $\gamma$ , a protein that controls the expression of genes. By stabilizing PPAR $\gamma$  and blocking its lysosomal degradation, the palmitoylation mechanism triggers the production of ACLY and subsequently leads to the development of lipid buildup-related CRC carcinogenesis

they are even more noteworthy. This intensifies our curiosity about the sample set and motivates us to investigate the underlying factors.

Aberrant expression or activation of associated enzymes leads to alterations in lipidome metabolic balance [51]. Currently, there is significant research being conducted on the involvement of zinc finger-aspartate-histidine-cysteine (DHHC)-CRD-type palmitoyl acyltransferases (ZDHHCs) in the stabilization of oncoproteins and their impact on the advancement of cancer. *Homo sapiens* and *Mus musculus* encode a combined total of 23 ZDHHCs. Multiple lines of evidence suggest that ZDHHCs have crucial functions in the process of lipogenesis [35, 52]. ZDHHC2 exhibits aberrant upregulation in renal cell carcinoma and plays a role in lipid production and carcinogenesis by modulating the ZDHHC2-AGK signaling axis [53]. ZDHHC18 functions as a palmitoyltransferase for MDH2, promoting the formation of ovarian cancer by maintaining mitochondrial respiration and reinstating the growth and clonogenic potential of ovarian cancer cells [54]. ZDHHC3 exacerbates the development of nonalcoholic steatohepatitis (NASH) and the progression of hepatocellular carcinoma (HCC) associated to NASH by boosting the accumulation of lipids regulated by IRHOM2 and the production of lipids mediated by FASN signaling [35]. Furthermore, we have discovered a distinct variation in the expression of ZDHHC6 between colorectal cancer (CRC) and normal tissues. Notably, this difference in ZDHHC6 expression exhibits a substantial association with ACLY and the biological processes associated to lipid production. ZDHHC6 acts as an oncogenic protein in the process of tumor formation. It is significantly upregulated in various types of malignancies, including CRC. ZDHHC6 exhibits an oncogenic role in conjunction with AEG-1 under specific circumstances. ZDHHC6 has also been identified as a predictive gene in the human pathology atlas. Prior research has shown the varied impacts of ZDHHC6 on biological mechanisms linked to the advancement of cancer [21]. ZDHHC6 plays a crucial function in cancer by exerting its impact on the growth and viability of cells. Evidence demonstrates that it stimulates the proliferation of cancerous cells by augmenting the functionality of growth factor receptors, such as epidermal growth factor receptor (EGFR) and platelet-derived growth factor receptor (PDGFR) [55, 56]. Furthermore, ZDHHC6 plays a vital role in palmitoylating the PI3K/Akt pathway, which is essential for cellular longevity and the ability to fight apoptosis [57, 58]. In addition, ZDHHC6 has the ability to regulate metastasis, which is a significant factor in cancer-related fatalities [14, 59]. It enhances the invasive and migratory properties of cancer cells via controlling the production and function of matrix metalloproteinases (MMPs) and focal adhesion kinase (FAK).

ZDHHC6 also participates in epithelial-mesenchymal transition (EMT), a biological mechanism linked to heightened metastatic capability. Moreover, ZDHHC6 has been discovered to influence angiogenesis, the process of creating new blood vessels that are necessary for the development of tumors [58, 60]. It enhances the release of pro-angiogenic substances such as vascular endothelial growth factor (VEGF), which stimulates the growth and creation of blood vessels by increasing the number of endothelial cells. Nevertheless, our findings indicate that ZDHHC6 facilitates the production of fatty acids from scratch in colorectal cancer (CRC). Furthermore, the atypical buildup of lipids induced by ZDHHC6 was partially reliant on the heightened expression of ACLY. ACLY, a pivotal enzyme regulating the production of new lipids, enhances the progression of CRC. Furthermore, the heightened expression of ACLY enhances the production of fatty acids and stimulates the formation of tumors. Our investigation revealed that specifically reducing the activity of ACLY significantly suppressed the promotion of tumor growth and the enhancement of fatty acid production induced by overexpression of ZDHHC6.

PPAR $\gamma$  is a crucial transcription factor that controls the production of lipids by increasing the transcription of enzymes involved in lipid synthesis, such as ACLY [61]. It exhibits significant expression in adipocytes and plays a role in the absorption, production, and retention of lipids. In this study, we discovered that PPAR $\gamma$  plays a role in the upregulation of ACLY by ZDHHC6 in the nucleus. Additionally, we showed that the palmitoylation of PPAR $\gamma$  by ZDHHC6 is essential for stabilizing PPAR $\gamma$  and allowing its incorporation into the nucleus. Increased expression of PPAR $\gamma$  stimulates the production of lipids and the development of tumors, together with the activation of ACLY in colorectal cancer (CRC). Our work discovered that ZDHHC6 may function as a precursor to ACLY. Nevertheless, regardless of the presence or absence of ACLY, ZDHHC6 still enhances the expression of PPAR $\gamma$ . Thus, ZDHHC6 has a role in stabilizing PPAR $\gamma$  regardless of ACLY expression, indicating that ZDHHC6 is involved in numerous regulatory pathways. Furthermore, during transportation to the cell nucleus, PPAR $\gamma$  can undergo several posttranslational changes that can impact its activity, stability, and interaction with other molecules. ZDHHC6's role in colon cancer lipid metabolism underscores a multifaceted regulatory mechanism that supports tumor growth and survival. Understanding the precise molecular interactions and pathways modulated by ZDHHC6-mediated palmitoylation will be essential for developing targeted therapies. Future research should focus on elucidating these mechanisms and exploring the therapeutic potential of ZDHHC6 inhibition in colon cancer treatment.

In summary, we demonstrate that ZDHHC6 stabilizes PPAR $\gamma$  through enhancing palmitoylation and greatly reducing its lysosomal degradation progress. The Cys-313 location at the DBD domain of PPAR $\gamma$  has been determined to be significant for the palmitoylation of PPAR $\gamma$  by ZDHHC6. PPAR $\gamma$  knockdown, in the meantime, eliminated the increase in ACLY expression and significantly reduced both carcinogenesis and fatty acid production induced by ZDHHC6 overexpression in CRC cells and xenograft tissues. Furthermore, patients who have colorectal cancer (CRC) and exhibit high expression levels of both ZDHHC6 and PPAR $\gamma$  tend to have an unfavorable prognosis and lower overall survival rates. To summarize, we have discovered a previously unknown signaling pathway called ZDHHC6-PPAR $\gamma$  pathway. This signaling is crucial in the process of lipid biosynthesis and CRC carcinogenesis. It also presents a potential target for cancer therapy that focuses on inhibiting fatty acid production.

#### Abbreviations

CRC	Colorectal cancer
ZDHHC6	Zinc finger DHHC-type palmitoyltransferase 6
ATCC	American Type Culture Collection
PPAR $\gamma$	Peroxisome proliferator-activated receptor gamma
FBS	Fetal bovine serum
IHC	Immunohistochemistry
TCGA	The cancer genome database
2- BP	3- 2-bromopalmitate
HA	Hyaluronic acid
CM	Cytomembrane
ACLY	ATP citrate lyase
SCD	Stearoyl-CoA desaturase
FASN	Fatty acid synthase
ICGC	International cancer genome consortium
GEO	Gene expression omnibus

#### Supplementary Information

The online version contains supplementary material available at <https://doi.org/10.1186/s13046-024-03154-0>.

Supplementary Material 1  
Supplementary Material 2  
Supplementary Material 3  
Supplementary Material 4  
Supplementary Material 5  
Supplementary Material 6  
Supplementary Material 7  
Supplementary Material 8  
Supplementary Material 9  
Supplementary Material 10  
Supplementary Material 11  
Supplementary Material 12  
Supplementary Material 13

#### Author contributions

Conceptualization & Methodology, Junqi Shan, Yanlai Sun; Investigation, Junqi Shan, Xinyu Li, Runqi Sun, Yao Yao, Yan Sun, Qin Kuang, Xianling Dai, Yanlai Sun; Data analysis, Junqi Shan, Xinyu Li, Runqi Sun, Yao Yao, Yanlai Sun; Funding acquisition, Project administration & Supervision, Yanlai Sun; Writing-original draft, Junqi Shan, Xinyu Li, Runqi Sun, Yanlai Sun; Writing review & editing, Junqi Shan, Xinyu Li, Yanlai Sun. All authors have read and approved the final manuscript.

#### Funding

This work was supported by (1) the Start-up fund of Shandong Cancer Hospital (NO. 2020PYA05); (2) the National Science Foundation of Shandong Province (NO. ZR2020MH254) and (3) the Science and Technology Program of Jinan (NO. 202134062).

#### Data availability

All data and material during the current study are available from the corresponding author on reasonable request.

#### Declarations

##### Ethics approval and consent to participate

The use of clinical samples was approved by the ethics committee of Shandong First Medical University & Shandong Academy of Medical Sciences and informed consent were obtained from all patients (ZR2020MH254). All animal experimental protocols were performed following the Ethical Animal Care and Use Committee of Shandong University (ZR2020MH254).

##### Consent for publication

All authors consent to the publication of this article.

##### Competing interests

The authors declare no competing interests.

##### Author details

<sup>1</sup>Department of Surgical Oncology, Shandong Cancer Hospital and Institute, Shandong First Medical University, Shandong Academy of Medical Sciences, Jinan, Shandong 250117, China

<sup>2</sup>School of Clinical Medicine, Shandong Second Medical University, Weifang, Shandong 261000, China

<sup>3</sup>School of Clinical Medicine, Jining Medical University, Jining, Shandong 272000, China

<sup>4</sup>Key Laboratory of Biorheological Science and Technology, Chongqing University, College of Bioengineering, Ministry of Education, Chongqing University, Chongqing 400030, PR China

Received: 20 April 2024 / Accepted: 4 August 2024

Published online: 16 August 2024

#### References

1. Siegel RL, et al. Colorectal cancer statistics, 2023. *Cancer J Clin.* 2023;73(3):233–54.
2. Morgan E et al. Global burden of colorectal cancer in 2020 and 2040: Incidence and mortality estimates from GLOBOCAN. *Gut* 72.2 (2023): 338–344.
3. Nadeem M, Shahid et al. Risk of colorectal cancer in inflammatory bowel diseases. *Seminars in cancer biology*. Vol. 64. Academic Press, 2020.
4. Bui TM et al. Tissue-specific reprogramming leads to angiogenic neutrophil specialization and tumor vascularization in colorectal cancer. *J Clin Investig* (2024).
5. Sanford NN, et al. Obesity and younger versus older onset colorectal cancer in the United States, 1998–2017. *J Gastrointest Oncol.* 2020;11(1):121.
6. Murphy CC, et al. Maternal obesity, pregnancy weight gain, and birth weight and risk of colorectal cancer. *Gut.* 2022;71(7):1332–9.
7. Ecker J et al. The colorectal cancer lipidome: identification of a robust tumor-specific lipid species signature. *Gastroenterology* 161.3 (2021): 910–923.
8. Wasinger VC, et al. Spp24 is associated with endocytic signalling, lipid metabolism, and discrimination of tissue integrity for 'leaky-gut' in inflammatory bowel disease. *Sci Rep.* 2020;10(1):12932.

9. Scalfani F, et al. Analysis of KRAS, NRAS, BRAF, PIK3CA and TP53 mutations in a large prospective series of locally advanced rectal cancer patients. *Int J Cancer*. 2020;146(1):94–102.
10. Martinelli E, et al. Implementing anti-epidermal growth factor receptor (EGFR) therapy in metastatic colorectal cancer: challenges and future perspectives. *Ann Oncol*. 2020;31(1):30–40.
11. Li W, et al. Insights into the post-translational modification and its emerging role in shaping the tumor microenvironment. *Signal Transduct Target Therapy*. 2021;6(1):422.
12. Lin X et al. Advances of Protein Palmitoylation in Tumor Cell Deaths. *Cancers* 15.23 (2023): 5503.
13. Bartolacci C, et al. Lipid metabolism regulates oxidative stress and ferroptosis in RAS-driven cancers: a perspective on cancer progression and therapy. *Front Mol Biosci*. 2021;8:706650.
14. Ko P-J, Scott J. Dixon. Protein palmitoylation and cancer. *EMBO Rep*. 2018;19:e46666.
15. Greaves J, Luke H. Chamberlain. DHHC palmitoyl transferases: substrate interactions and (patho) physiology. *Trends Biochem Sci*. 2011;36:245–53.
16. Stix R, et al. Structure and mechanism of DHHC protein acyltransferases. *J Mol Biol*. 2020;432:4983–98.
17. Gao T, et al. Recent progress of palmitoyl transferase DHHC3 as a novel antitumor target. *Future Med Chem*. 2022;14(6):443–55.
18. Salaun C, Nicholas CO, Tomkinson, Luke H. Chamberlain. The endoplasmic reticulum-localized enzyme zDHHC6 mediates S-acylation of short transmembrane constructs from multiple type I and II membrane proteins. *J Biol Chem*. 2023;299:10.
19. Fhu CW, Ali A. Protein lipidation by palmitoylation and myristoylation in cancer. *Front Cell Dev Biology*. 2021;9:673647.
20. Zhang Y, et al. Oxidized high-density lipoprotein promotes CD36 palmitoylation and increases lipid uptake in macrophages. *J Biol Chem*. 2022;298:6.
21. Zhou B et al. The palmitoylation of AEG-1 dynamically modulates the progression of hepatocellular carcinoma. *Theranostics* 12.16 (2022): 6898.
22. Fredericks GJ et al. Stable expression and function of the inositol 1, 4, 5-triphosphate receptor requires palmitoylation by a DHHC6/selenoprotein K complex. *Proceedings of the National Academy of Sciences* 111.46 (2014): 16478–16483.
23. Marciel MP, Peter R. Hoffmann. Molecular mechanisms by which selenoprotein K regulates immunity and cancer. *Biol Trace Elem Res*. 2019;192:60–8.
24. Pagano C, et al. Advances in adiponcosis: insights in the inner mechanisms at the base of adipose and tumour tissues interplay. *Int J Cancer*. 2023;152(12):2464–73.
25. Wagner N, Kay-Dietrich Wagner. PPAR beta/delta and the hallmarks of cancer. *Cells* 9.5 (2020): 1133.
26. Cheng H, Sheng et al. PPARs and tumor microenvironment: the emerging roles of the metabolic master regulators in tumor stromal-epithelial crosstalk and carcinogenesis. *Cancers* 13.9 (2021): 2153.
27. Morigny P, et al. Lipid and glucose metabolism in white adipocytes: pathways, dysfunction and therapeutics. *Nat Reviews Endocrinol*. 2021;17(5):276–95.
28. Faghfoury A, Hossein, et al. PPAR-gamma agonists: potential modulators of autophagy in obesity. *Eur J Pharmacol*. 2021;912:174562.
29. Salita T et al. Reprogrammed lipid metabolism and the lipid-associated hallmarks of colorectal cancer. *Cancers* 14.15 (2022): 3714.
30. Pan S, et al. Therapeutic potential of melatonin in colorectal cancer: focus on lipid metabolism and gut microbiota. *Biochim et Biophys Acta (BBA)-Molecular Basis Disease*. 2022;1868(1):166281.
31. Jin X et al. Pathophysiology of obesity and its associated diseases. *Acta Pharm Sinica B* (2023).
32. Wang D et al. Crosstalk between peroxisome proliferator-activated receptor  $\delta$  and VEGF stimulates cancer progression. *Proceedings of the National Academy of Sciences* 103.50 (2006): 19069–19074.
33. You M et al. PPAR $\delta$  signaling regulates colorectal cancer. *Current pharmaceutical design* 21.21 (2015): 2956–2959.
34. Lin M, Song, et al. Expression of PPAR $\gamma$  and PTEN in human colorectal cancer: an immunohistochemical study using tissue microarray methodology. *Oncol Lett*. 2011;2:1219–24.
35. Xu M, et al. Palmitoyltransferase ZDHHC3 aggravates nonalcoholic steatohepatitis by Targeting S-Palmitoylated IRHOM2. *Adv Sci*. 2023;10:2302130.
36. Tan HW, Siong, et al. Lysosomal inhibition attenuates peroxisomal gene transcription via suppression of PPARA and PPARGC1A levels. *Autophagy*. 2019;15:1455–9.
37. Videira NatáliaB et al. PPAR modulation through posttranslational modification control. *Nuclear Receptors: Art Sci Modulator Des Discovery* (2021): 537–611.
38. Scholtes C, Giguère V. Transcriptional control of energy metabolism by nuclear receptors. *Nat Rev Mol Cell Biol*. 2022;23(11):750–70.
39. Wadosky KM, Monte S. Willis. The story so far: post-translational regulation of peroxisome proliferator-activated receptors by ubiquitination and SUMOylation. *Am J Physiol Heart Circ Physiol*. 2012;302(3):H515–26.
40. Porcuna Jesús, Mínguez-Martínez J. The PPAR $\alpha$  and PPAR $\gamma$  epigenetic landscape in cancer and immune and metabolic disorders. *Int J Mol Sci*. 2021;22:10573.
41. Chinetti-Gbaguidi G, et al. Peroxisome proliferator-activated receptor  $\alpha$  controls cellular cholesterol trafficking in macrophages. *J Lipid Res*. 2005;46(12):2717–25.
42. Chen D, et al. A Multidimensional characterization of E3 ubiquitin ligase and substrate Interaction. *Netw iScience*. 2019;16:177–91.
43. Visweswaran M, et al. Aberrant lipid metabolism as an emerging therapeutic strategy to target cancer stem cells. *Stem Cells*. 2020;38(1):6–14.
44. Mahmud I et al. DAXX drives de novo lipogenesis and contributes to tumorigenesis. *Nature communications* 14.1 (2023): 1927.
45. Mozolewska P, et al. Inhibitors of fatty acid synthesis and oxidation as potential anticancer agents in colorectal cancer treatment. *Anticancer Res*. 2020;40(9):4843–56.
46. Qiao C, et al. IGF1-mediated HOXA13 overexpression promotes colorectal cancer metastasis through upregulating ACLY and IGF1R. *Cell Death Dis*. 2021;12(6):564.
47. Schulz-Kuhnt A et al. ATP citrate lyase (ACLY)-dependent immunometabolism in mucosal T cells drives experimental colitis in vivo. *Gut* (2024).
48. Broadfield LA, et al. Lipid metabolism in cancer: new perspectives and emerging mechanisms. *Dev Cell*. 2021;56(10):1363–93.
49. Beloribi-Djefafilia S, Vasseur S, Guillaumond F. Lipid metabolic reprogramming in cancer cells. *Oncogenesis*. 2016;5(1):e189–189.
50. Krauß D, Fari O, Sibilia M. Lipid Metabolism Interplay CRC—An Update *Metabolites*. 2022;12(3):213.
51. Fernández LP, Marta Gomez De Cedron, and Ana Ramirez De Molina. Alterations of lipid metabolism in cancer: implications in prognosis and treatment. *Front Oncol*. 2020;10:577420.
52. Wang J, et al. DHHC4 and DHHC5 facilitate fatty acid uptake by palmitoylating and targeting CD36 to the plasma membrane. *Cell Rep*. 2019;26(1):209–21.
53. Sun Y, et al. ZDHHC2-Mediated AGK palmitoylation activates AKT-mTOR signaling to reduce Sunitinib Sensitivity in Renal Cell Carcinoma. *Cancer Res*. 2023;83(12):2034–51.
54. Pei X, et al. Palmitoylation of MDH2 by ZDHHC18 activates mitochondrial respiration and accelerates ovarian cancer growth. *Sci China Life Sci*. 2022;65(10):2017–30.
55. Coronel Arrechea, Consuelo, et al. A novel yeast-based high-throughput method for the identification of protein palmitoylation inhibitors. *Open Biology*. 2021;11:200415.
56. Tecik M, Adan A. Therapeutic targeting of FLT3 in acute myeloid leukemia: current status and novel approaches. *OncoTargets Therapy* (2022): 1449–78.
57. Lin H. Protein cysteine palmitoylation in immunity and inflammation. *FEBS J*. 2021;288(24):7043–59.
58. Zhou B, et al. Protein palmitoylation in cancer: molecular functions and therapeutic potential. *Mol Oncol*. 2023;17(1):3–26.
59. Qu M, et al. Lipid-induced S-palmitoylation as a vital regulator of cell signaling and disease development. *Int J Biol Sci*. 2021;17:4223.
60. Wu Z, et al. Protein S-Palmitoylation and Lung diseases. *Lung inflammation in Health and Disease*, volume II. Cham: Springer International Publishing; 2021. pp. 165–86.
61. Noh K, Hee, et al. Ubiquitination of PPAR-gamma by pVHL inhibits ACLY expression and lipid metabolism, is implicated in tumor progression. *Metabolism*. 2020;110:154302.

## Publisher's Note

Springer Nature remains neutral with regard to jurisdictional claims in published maps and institutional affiliations.